Research Article

AllBRICQS: The All-sky BRIght, Complete Quasar Survey

Christopher A. Onken[1], Christian Wolf[1,2], Wei Jeat Hon[3], Samuel Lai (赖民希)[1], Patrick Tisserand[4], and Rachel Webster[3]
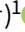
[1]Research School of Astronomy and Astrophysics, Australian National University, Canberra ACT 2611, Australia, [2]Centre for Gravitational Astrophysics, Australian National University, Canberra ACT 2600, Australia, [3]School of Physics, University of Melbourne, Parkville, VIC 3010, Australia and [4]Sorbonne Universités, UPMC Univ Paris 6 et CNRS, Institut d'Astrophysique de Paris, 98 bis bd Arago, F-75014 Paris, France

Abstract

We describe the first results from the All-sky BRIght, Complete Quasar Survey (AllBRICQS), which aims to discover the last remaining optically bright quasars. We present 156 spectroscopically confirmed quasars (140 newly identified) having $|b| > 10°$. 152 of the quasars have *Gaia* DR3 magnitudes brighter than $B_P = 16.5$ or $R_P = 16$ mag, while four are slightly fainter. The quasars span a redshift range of $z = 0.07 - 3.93$. In particular, we highlight the properties of J0529-4351 at $z = 3.93$, which, if unlensed, is one of the most intrinsically luminous quasars in the Universe. The AllBRICQS sources have been selected by combining data from the *Gaia* and *WISE* all-sky satellite missions, and we successfully identify quasars not flagged as candidates by *Gaia* Data Release 3. We expect the completeness to be ≈96% within our magnitude and latitude limits, while the preliminary results indicate a selection purity of ≈96%. The optical spectroscopy used for source classification will also enable detailed quasar characterisation, including black hole mass measurements and identification of foreground absorption systems. The AllBRICQS sources will greatly enhance the number of quasars available for high-signal-to-noise follow-up with present and future facilities.

Keywords: active galactic nuclei: quasars; supermassive black holes

1. Introduction

Optically bright quasars represent an admixture of sources drawn from a continuum of properties—at one extreme: the rare, distant, rapidly growing black holes (BHs); and at the other: the more common, modestly growing BHs located closer to the Milky Way. Previous work has found the cumulative surface density of optically bright quasars to be well described by a power-law as a function of magnitude, such that the integrated number of quasars brighter than $B_J = 15.5$ mag is 1 per 100 deg², and increases by 1 dex for every 1.3 mag of decreased optical flux (Wisotzki et al. 2000).

Compared to the bulk of quasars at fainter optical magnitudes, the bright end of the distribution offers obvious advantages in terms of signal-to-noise for detailed follow-up. Such quasars are particularly useful as background sources for studies of intervening absorption from circumgalactic (Tumlinson, Peeples, & Werk 2017) and intergalactic gas (McQuinn 2016).

Moreover, because the physical size of the quasar broad-line region (BLR) scales with luminosity as $\sim \sqrt{L}$ (Bentz et al. 2013), and, to first order, the distance to the quasar scales as $\sqrt{L/F}$ for flux F, the *angular* size of the BLR scales as $\sqrt{F}$. This means that the optically brightest quasars have the largest apparent BLRs, making them especially interesting targets for high spatial resolution investigation with instruments such as GRAVITY on the Very Large Telescope Interferometer (VLTI; e.g., Gravity Collaboration et al. 2018, 2020, 2021b,a).

Approximately 1% of spectroscopically confirmed active galactic nuclei (AGNs)[a] have *Gaia* Data Release 3 photometry (Gaia Collaboration 2016, 2021) brighter than $B_P = 16.5$ or $R_P = 16$ mag, and 89% of those bright objects have redshifts less than $z = 0.1$. The recent discovery of a remarkably bright quasar at $z = 0.83$—SMSS J114447.77-430859.3 (hereafter, J1144-4308), with $B_P = 14.64$ mag (Onken et al. 2022a)—motivates a renewed search for other bright quasars that have gone undetected.

Here we describe the search criteria and first results from the All-sky BRIght, Complete Quasar Survey (AllBRICQS). In Section 2, we explain the AllBRICQS selection criteria. In Section 3, we describe the optical spectroscopy obtained for the first set of candidates. We present the spectroscopically confirmed AllBRICQS sample in Section 4 and report on our preliminary success rate. In Section 5, we examine the highest-redshift AllBRICQS discovery, J0529-4351, in greater detail. Section 6 compares our confirmed quasars with the quasar catalogues derived from *Gaia* DR3. In Section 7, we discuss the present results and the outlook for the scientific exploitation of the completed survey.

We adopt a flat ΛCDM cosmology, having a matter density of $\Omega_m = 0.3$ and a Hubble-Lemaître constant of $H_0 = 70$ km s^{-1} Mpc^{-1}. Throughout the paper, we use Vega magnitudes unless otherwise specified.

[a]These statistics are based on the Million Quasars Catalogue (Flesch 2021), version 7.6; hereafter, Milliquas.
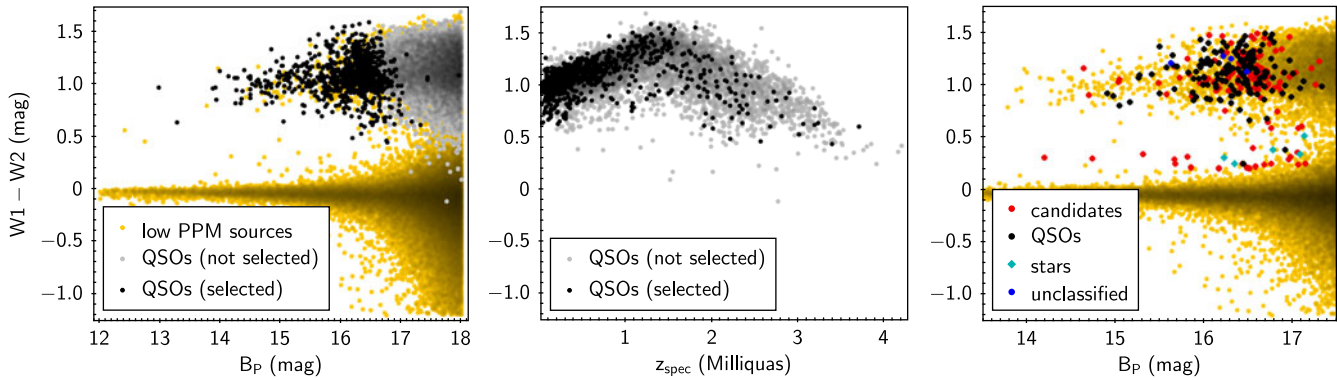
Figure 1. Left panel: *WISE* $W1 - W2$ colour versus *Gaia* B_P magnitude of objects with low parallax and proper motion (yellow); known quasars are shown in black or, if they violate our selection criterion, in grey. Centre panel: $W1 - W2$ colour versus redshift for known quasars satisfying (black) or violating (grey) our selection criteria. Right panel: $W1 - W2$ colour versus B_P magnitude for objects with low PPM in yellow, the new AllBRICQS quasars in black, contaminating stars in cyan, unclassified spectra in blue, and unobserved candidates in red.

2. Candidate selection

Finding bright quasars has been greatly simplified in modern times, first with the all-sky survey of the *Wide-field Infrared Survey Explorer* (*WISE; Wright et al. 2010; Mainzer et al. 2014*), and more recently with the accurate parallax and proper motion information from the all-sky survey of *Gaia*. Several authors have proposed very effective methods for selecting quasar candidates exploiting these data sets using hard selection cuts, Bayesian probabilities, or machine-learning approaches (e.g., Calderone et al. 2019; Shu et al. 2019; Wolf et al. 2020). Here, we choose a very simple approach, given that we focus our interest at bright magnitudes, where the stars, galaxies, and quasars can be easily separated, as demonstrated below.

We avoid the vicinity of the Galactic Plane, where quasars are dimmed by dust extinction and are harder to identify reliably due to source crowding biasing the photometry, especially in the *WISE* catalogue, where the large point spread function in the infrared passbands leads to blending. Effective searches in the Galactic Plane include the work of Fu et al. (2022), who have recently discovered 191 new quasars, five of which are brighter than $i = 16$ ABmag. In contrast, we restrict our search to a Galactic latitude of $|b| > 10°$ and avoid the most difficult parts of the plane.

Previous work has shown that known quasars have *Gaia* parallaxes and proper motions (PPM) that are statistically consistent with zero within their errors (e.g., Liao et al. 2021; Onken et al. 2022b; Souchay et al. 2022, but for interesting counter-examples, see Wu et al. 2022) and hence we restrict the search to a target list with parallaxes and proper motions of low ($<4\sigma$) significance. We also restrict the search to objects with a *Gaia* B_P/R_P excess factor (phot_bp_rp_excess_factor; see Riello et al. 2021) <1.5, which rejects clearly extended or blended sources. Among the known broad-line quasars in the Milliquas catalogue having *Gaia* $B_P < 17$ mag, $z > 0.3$, and $|b| > 10°$, the selection rules above reject less than 4% of the quasars (43 out of 1227); some of the rejected objects have no PPM measurements at all, however, the vast majority of the objects are simply consistent with being drawn from the tails of a zero-PPM population.

We investigated several colour properties, and found that the mid-infrared $W1 - W2$ colour provides a highly effective distinction between the known quasars and the bulk of the candidate sample, which are primarily distant (hence, small PPM) stars. In the left panel of Figure 1, we show the $W1 - W2$ colour vs *Gaia* B_P magnitude for the known quasars from Milliquas and the sample

passing the *Gaia* criteria above. At $B_P < 17$ mag, the quasar and non-quasar population appear clearly separated, while they start to blend into each other at fainter magnitudes. As the known quasars have been compiled from a variety of selection methods (X-ray, UV, optical, radio), the mid-infrared quasar colours should not be subject to any particular biases beyond the scatter arising from the photometric errors, and just reflect the typical spectral energy distribution (SED) associated with accretion onto a BH. Thus, we select quasar candidates using the simple rule of $W1 - W2 > 0.2$ mag. While there is likely to be increasing contamination towards that $W1 - W2$ boundary, the moderate number of candidates to follow-up allows us to pursue a strategy that emphasises completeness (and the threshold may be relaxed further in future expansions of the observing campaign). Based on the PPM statistics above, expect the completeness to be $\approx 96\%$ for $|b| > 10°$.

As shown in the middle panel of Figure 1, the quasars that approach our $W1 - W2$ threshold at faint B_P magnitudes are strongly biased towards high redshift, but some sources at $z \sim 4$ can still be found within our selected region.

We limit the present sample to have either $B_P < 16.5$ or $R_P < 16$ mag and find 290 candidates[b] (see right panel of Figure 1). Approximately 500 broad-line quasars are known at $z > 0.3$ within these magnitude limits. If $\sim 85\%$ of our candidates were similar objects, then one third of bright quasars would be missing from current catalogues and be revealed by AllBRICQS.

In Figure 2 we characterise our candidate list further in relation to known quasars of similar brightness. We can see that our new candidates are more numerous at Southern declinations and especially at Southern Galactic latitudes. The reason is, of course, that the Sloan Digital Sky Survey (SDSS, York et al. 2000; Richards et al. 2002; Abdurro'uf & et al. 2022), which has revealed a huge sample of quasars, was focused on the Northern Galactic Cap.

3. Observations and data processing

Optical spectroscopy was obtained with the Australian National University (ANU) 2.3-m telescope at Siding Spring Observatory (SSO) using the Wide Field Spectrograph (WiFeS; Dopita et al.

---

[b]An early version of the sample definition extended the depth a further 0.5 mag, and we present four quasars discovered from that sample in Tables A.1 and E.1, as well as the spectrum gallery in Appendix B.
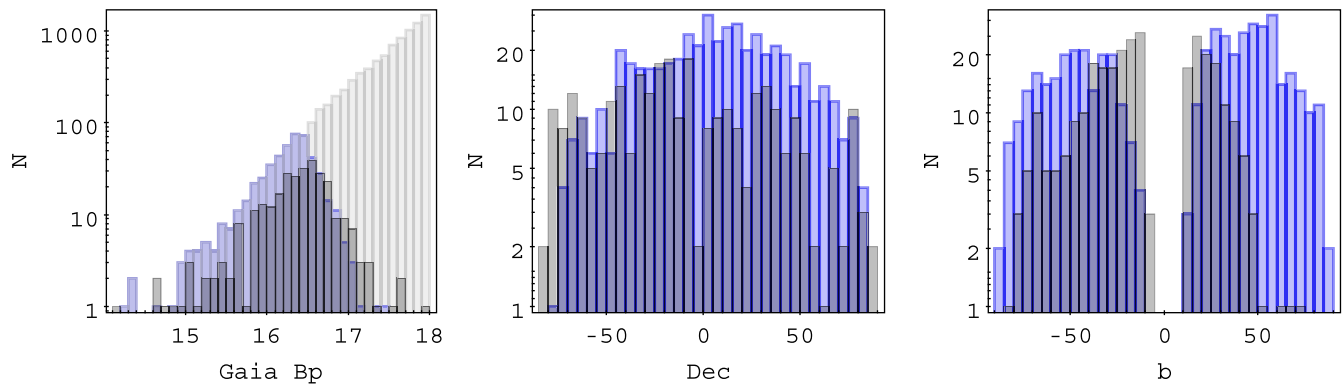
Figure 2. Number counts of AllBRICQS candidates (dark grey) as a function of *Gaia B_P* magnitude (left), declination (centre), and Galactic latitude (right). The blue histograms are known quasars for the same magnitude range as the candidates: *Gaia B_P* < 16.5 or R_P < 16 mag. Light grey are all known quasars.

2007, 2010). WiFeS is an integral field spectrograph and, with a spatial binning of 2 pixels, provides $1 \times 1''$ sampling over a $25 \times 38''$ field-of-view.

WiFeS spectra were obtained between UT 2022 March 11 and 2022 November 24 for the AllBRICQS sample presented here. We note that observations on one of those nights (UT 2022 June 14) were conducted as part of the Science Verification activities for the fully robotic operations of the ANU 2.3 m telescope. The targets were selected from the candidate list based purely on considerations of observability (Right Ascension and airmass), aiming for complete coverage of the list (between RA=10 h and 5 h, only five candidates still needed observing).

With the resolving power $R \sim 3000$ gratings and the RT560 beamsplitter, we used exposure times between 180 and 1500 s, covering the wavelength range 3250–9550 Å across the two cameras of the spectrograph. Various spectrophotometric standard stars were observed alongside the AllBRICQS candidates and were used for calibrating the overall spectral shape. However, because the standards were not necessarily observed under the same observing conditions, we do not utilise them for absolute flux calibration.

The raw data were processed with the PYTHON-based pipeline, PyWiFeS (Childress et al. 2014). We then extracted the spectra from the 3D data cubes (separate cubes for each arm of the spectrograph) using QFITSVIEW,[c] utilising nearby regions for sky subtraction. The signal-to-noise values in the final spectra were typically between 10 and 50 per pixel.

The spectra were classified and redshifted by eye, aided by the MARZ online application[d] (Hinton et al. 2016; Hinton 2016). The typical redshift uncertainty is 0.01, but can be either better or worse depending on the details of the available emission lines and their shapes.

4. AllBRICQS sample

The observations reported here encompass 166 of the 290 AllBRICQS candidates. We present a list of the 156 confirmed AllBRICQS quasars in Appendix A, arranged in order of ascending RA. A gallery of the quasar spectra, arranged in order of ascending redshift, is provided in Appendix B. Four unclassified sources are presented in Appendix C. Finally, the six stars we observed are presented in Appendix D.

[c]Available from https://www.mpe.mpg.de/~ott/QFitsView/.
[d]See http://samreay.github.io/Marz.

As noted in Appendix A, 140 of our 156 quasars represent new discoveries, while the remaining 16 are composed of quasars identified from the Edinburgh-Cape Blue Object Survey (13 quasars without published redshifts, and so intentionally retained in the candidate list; Stobie et al. 1997; Kilkenny et al. 2016); two quasars of known redshift, but lacking published optical spectroscopy; and one quasar announced since the beginning of the AllBRICQS observing campaign. In contrast, just six candidates have proven to be stars. Excluding the four quasars beyond our *Gaia* magnitude limits and the four unclassified sources, this gives a preliminary estimate of the AllBRICQS selection purity of 152/158 = 96%.

The right panel of Figure 1 suggests that the purity is declining at the blue end of the $W1 - W2$ range, but we do find quasars near the boundary and will wait for the completed sample before making a more comprehensive statistical analysis.

4.1. Luminosities

We flux-calibrate the WiFeS spectra for the AllBRICQS quasars with the *Gaia* DR3 B_P and R_P photometry and then correct for Galactic extinction using the Fitzpatrick et al. (2019) extinction curve implemented in the dust_extinction PYTHON package (Gordon 2021). We assume $R_V = 3.1$, and apply a $\times 0.86$ correction factor to the values drawn from the Schlegel, Finkbeiner, & Davis (1998) $E(B - V)$ map (Schlafly & Finkbeiner 2011). We derive continuum luminosities from the observed redshifts and the median extinction-corrected emission in 20 Å windows centred around the rest-frame wavelengths of 1450, 3000, and 5100 Å (as the redshifts permit, and excluding the 1450 Å continuum for broad absorption line quasars). We also estimate the bolometric luminosity for each quasar by applying the bolometric corrections (BCs) from Runnoe, Brotherton, & Shang (2012b,a) and adopting the mean when multiple values are available. The continuum and bolometric luminosities are provided in Appendix E. Based on the typical RMS fluxes within the spectroscopic continuum windows, we expect the luminosity estimates to be reliable at the level of 0.1 dex, but plan to make more precise measurements when performing detailed spectral fitting in future work.

The bolometric luminosities across redshift are shown in comparison to the quasars from the 14th data release of SDSS (DR14Q; Rakshit, Stalin, & Kotilainen 2020) in Figure 3. To adopt a consistent bolometric correction as above, we apply the Runnoe et al. (2012b,a) BCs to the tabulated DR14Q continuum luminosities
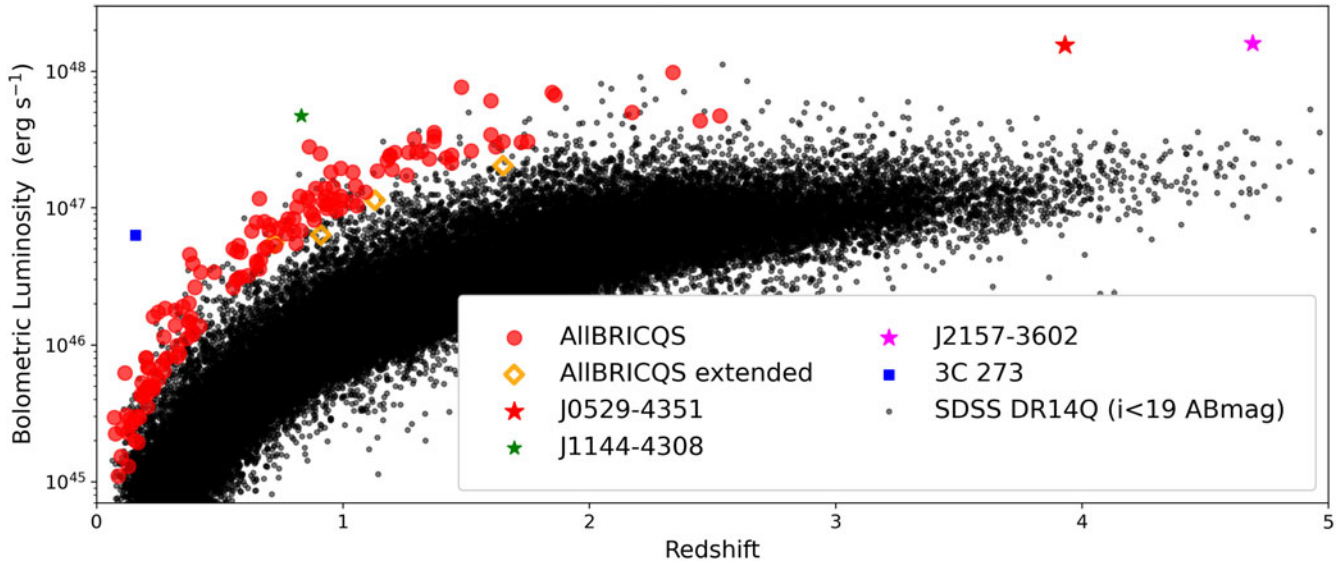
Figure 3. Bolometric luminosity versus redshift for the first AllBRICQS quasars (red circles), with the highest-redshift source (J0529-4351; see Section 5) indicated as a red star. The AllBRICQS discoveries that are fainter than $B_P = 16.5$ and $R_P = 16$ mag are indicated with open orange diamonds. For comparison, we also show 3C 273 (blue square); the recently discovered J1144-4308 (green star; Onken et al. 2022a); the most luminous known quasar, J2157-3602 (magenta star; Wolf et al. 2018a; Onken et al. 2020); and the numerous quasars observed by SDSS grey points; (grey points; Rakshit et al. 2020). The AllBRICQS quasars improve our knowledge of the luminous end of the quasar distribution across a wide redshift range.

and again take the mean value when multiple estimates are available. We also show in Figure 3 a number of bright quasars for comparison with the AllBRICQS sample: the long-studied 3C 273; the most luminous known quasar in the Universe, SMSS J215728.21-360215.1 (hereafter, J2157-3602; Wolf et al. 2018a; Onken et al. 2020); and the bright quasar which inspired the AllBRICQS project, J1144-4308 (Onken et al. 2022a). The AllBRICQS quasars fill a niche not well populated by the DR14Q sample, despite substantial overlap between the SDSS bright-end limit of $i_{SDSS} = 15$ ABmag and the AllBRICQS faint-end limit of $R_P = 16$ mag ($i_{SDSS} \approx 16.35$ ABmag).

For the extended AllBRICQS sample (having *Gaia* magnitudes just fainter than our main sample's criteria of $B_P < 16.5$ mag or $R_P < 16$ mag), we find one quasar, J1501-1053 at $z = 0.72$, with a luminosity that places it amongst the bulk of the AllBRICQS population (5.5×10^{46} erg s^{-1}). This quasar is relatively blue ($B_P - R_P=0.59$ mag), yet is in the 74th percentile of reddening amongst our confirmed quasars, with an $E(B - V)_{SFD}=0.12$ mag. The extinction-corrected continuum luminosities at both 3000 and 5100 Å provide a consistent estimate of the bolometric luminosity, indicating that it was the foreground dust that caused the source to be marginally outside our selection criteria.

4.2. Gravitational lensing

One mechanism for producing high apparent luminosities is gravitational lensing, but we do not find evidence that the AllBRICQS sample is significantly affected by such magnifications. Here, we describe the general findings for the AllBRICQS sample, with particular discussion of the $z = 3.93$ quasar, J0529-4351, deferred to Section 5.

First, we have visually inspected the optical images available from the SkyMapper Southern Survey[e] (Wolf et al. 2018b; Onken

et al. 2019), the Pan-STARRS1 Survey[f] (Chambers et al. 2016; Waters et al. 2020), and the Dark Energy Camera (DECam) archive[g] (Flaugher et al. 2015; Valdes, Gruendl, & DES Project 2014), and find no indications of small-separation point sources that would be consistent with being multiple, lensed images of the quasar (although the low-redshift quasars often have visible host galaxies, including three—J0400-2257, J1619-7832, and J2126-4529—which appear to be hosted by one component of a major galaxy merger).

Furthermore, we have examined the properties of the AllBRICQS quasars in the catalogues of the DECam Local Volume Exploration Survey (DELVE) DR2 (Drlica-Wagner et al. 2022) and the NOIRLab Source Catalog (NSC) DR2 (Nidever et al. 2021). In neither catalogue do we find any AllBRICQS sources at $z > 0.5$ with significant evidence of being spatially extended.

Taking advantage of the spatial resolution of *Gaia*, we also computed the C^* statistic of Riello et al. (2021), which corrects the phot_bp_rp_excess_factor for colour-based trends. The C^* values compare the fluxes in the wide-aperture spectroscopic windows (B_P and R_P) with the narrow-aperture astrometric window (G-band), and are constructed to be 0 for point sources. Comparing the C^* values with their expected (G-magnitude-based) uncertainties, we find the vast majority of high C^*/σ quasars are the low redshift quasars in which the host galaxy is expected to contribute significant flux. At $z > 0.5$, only 9% (9 of 96 quasars) have $C^*/\sigma > 2$, and 2% (2 quasars: J0117-1712 at $z = 0.68$, and J0530+0042 at $z = 0.7$) have $C^*/\sigma > 3$. For the $>3\sigma$ quasars, the former has deep imaging by the Dark Energy Survey (Abbott et al. 2021) that shows a source 1.5″ away. However, the *Gaia* DR3 astrometry for this $G = 19.71$ mag neighbour reveals it to be a foreground star. Meanwhile, J0530+0042 has DECam imaging (NOIRLab Prop. ID 2014B-0193; PI: F. Walter), which

shows a faint source ($\sim$20.5 ABmag in $i-$ and z-band), 3.5$''$ to the Northeast, which is not catalogued by *Gaia* DR3, DELVE DR2, or NSC DR2. As this neighbour is beyond the 3.5-arcsec-wide B_P/R_P aperture, the relation to the high C^* value is unclear, but we conclude that there is no convincing evidence for a foreground lens.

The lack of multiply imaged quasars is likely a consequence of our selection criteria. Requiring phot_bp_rp_excess_factor <1.5 would eliminate $\sim$65% of the known gravitational lenses from either the Gravitationally Lensed Quasar Database[h] (see Lemon, Auger, & McMahon 2019) or from a recent compilation of lensed, binary, and projected quasar pairs (Lemon et al. 2022). Additional lensing systems are likely to be lost from the AllBRICQS candidate list by violation of our $W1 - W2$ criterion through the mid-IR contributions from the lensing galaxy.

Thus, we find that the AllBRICQS quasars presented here are intrinsically luminous sources, drawn from the bright end of the quasar luminosity function.

5. The case of J0529-4351

In this section, we focus on the properties of the $z = 3.93$ quasar, J0529-4351. As indicated in Figure 3, the continuum flux at rest-frame 1450 Å suggests an intrinsic bolometric luminosity of 1.5×10^{48} erg s^{-1}, on par with the most luminous known quasar, J2157-3602 (Wolf et al. 2018a; Onken et al. 2020). In the observed frame, aside from two gravitationally lensed systems (APM 08279+5255 and B 1422+231), J0529-4351 has the brightest *Gaia* R_P magnitude of any quasar more distant than HS 1946+7658 at $z = 3.051$. Hence, we examine in detail the available imaging data to constrain the possibility of gravitational lensing boosting the observed flux.

As discussed in Section 4.2, the relative flux measured by *Gaia* through its narrow (G-band) and wide (B_P and R_P) apertures can be used as a measure of extended emission on sub-arcsecond spatial scales. For J0529-4351, the colour-corrected phot_bp_rp_excess_factor, C^*, is found to be -0.037. With the 1σ scatter expected to be 0.02 at $G = 16.34$ mag (Riello et al. 2021), the *Gaia* data do not indicate any additional flux at radii larger than 0.175$''$ from the quasar (half the 0.35$''$ aperture of the G-band).

In addition, the Dark Energy Survey (DES) DR2 (Abbott et al. 2021) photometry for J0529-4351 is found to be consistent with a point source in all five optical/infrared bands ($grizY$): the SPREAD_MODEL and WAVG_SPREAD_MODEL are below 0.001 (where values below 0.003 have been found to robustly isolate stellar sources in $griz$ imaging of similar depth; Desai et al. 2012), and the CLASS_STAR estimates are >0.98.

To assess possible microlensing of J0529-4351 from stars in a putative foreground galaxy, we examined the photometry from several surveys of the past decade. SMSS DR3 optical photometry[i] indicates a dimming of ~ 0.2 mag between 2014 November and 2019 October in $griz$ (the source is undetected in the u and v filters because of the Lyα absorption). Similarly, the photometry from the NEOWISE 2022 Data Release[j] (Mainzer et al. 2014) in $W1$ and $W2$, obtained between 2014 March and 2021 September, indicates no more than 0.05 mag of dimming over that time span.

In terms of large-separation lensed images, the only other *Gaia* DR3 source in a 30$'$ search radius having similar colours, low PPM, and an R_P within 2 mag of J0529-4351 is shown by DES imaging to be the centre of a foreground spiral galaxy.

We find that the existing data for J0529-4351 provides no evidence that the quasar is gravitationally lensed, and thus, we conclude that its extraordinary luminosity is likely to be an indication of an extremely high accretion rate onto its BH.

In terms of its multi-wavelength properties, we find no radio detections within 2$'$ in DR1 of the Rapid ASKAP Continuum Survey (RACS; McConnell et al. 2020; Hale et al. 2021), and no X-ray counterparts catalogued within 25$'$ in the Second *ROSAT* all-sky X-ray Survey (2RXS; Boller et al. 2016).

Given the unusual nature of J0529-4351, we have already begun to collect additional data to further investigate this remarkable quasar.

6. Comparison with *Gaia*-selected quasars

We compare our confirmed quasars with the quasar catalogues derived from the *Gaia* variability analysis (Carnerero et al. 2022), or from other *Gaia* source classification methods (Gaia Collaboration 2022; Delchambre et al. 2022), including those utilising the B_P/R_P low-resolution spectra (De Angeli et al. 2022; Montegriffo et al. 2022).

First, we consider the *Gaia* DR3 variabLE AgN sample (GLEAN; Carnerero et al. 2022). The GLEAN coverage excludes the Galactic Plane and regions around the Magellanic Clouds because of its constraint on the number density of sources within 100 arcsec being less than 0.004 arcsec^{-2}. This irregular exclusion zone covers $|b| \lesssim 25°$ at the Galactic Centre, but allows sparse sampling of the Plane in the direction of the Anti-centre. The GLEAN sample[k] totals over 872000 sources, including more than 21000 potentially new quasars. The latter are predominantly at $G_P > 20$ mag, significantly fainter than the AllBRICQS regime ($G_P \lesssim 17$ mag).

We indicate in Table A.1 whether each AllBRICQS quasar was included in the GLEAN sample, or in another *Gaia* DR3 variability table,[l] or neither. The completeness of the GLEAN sample is estimated (cf. Figure 24 of Carnerero et al. 2022) to be >80% for $G_P < 17$ mag, with a purity of >95%. Having 123 of our 156 quasars selected by GLEAN, and one GLEAN-selected star compared to the 123 quasars, the first AllBRICQS sample is consistent with the Carnerero et al. (2022) estimates.

We further compare the AllBRICQS quasars to the classifications produced by *Gaia*'s Discrete Source Classifier (DSC; Gaia Collaboration 2022; Delchambre et al. 2022), a probabilistic classification algorithm that was trained on 300000 SDSS quasars. The DSC assigned a quasar label (via the Combmod classifier, recorded in the classlabel_dsc parameter) to 116 of our 156 quasars, or 74% completeness within the present sample. This appears to be significantly lower than the expected[m] quasar completeness for $G_P < 17$ mag of nearly 100%. We find that 37 of the AllBRICQS quasars were labelled as stars (including one as a 'physicalbinary'), as was just 1 of the 6 stars we observed. Of particular note, J0529-4351,

---

[h] See https://research.ast.cam.ac.uk/lensedquasars/.

[i] SMSS DR3 is currently available to Australian astronomers, but the upcoming SMSS DR4 will be rapidly made available to astronomers worldwide.

[j] See https://wise2.ipac.caltech.edu/docs/release/neowise/.

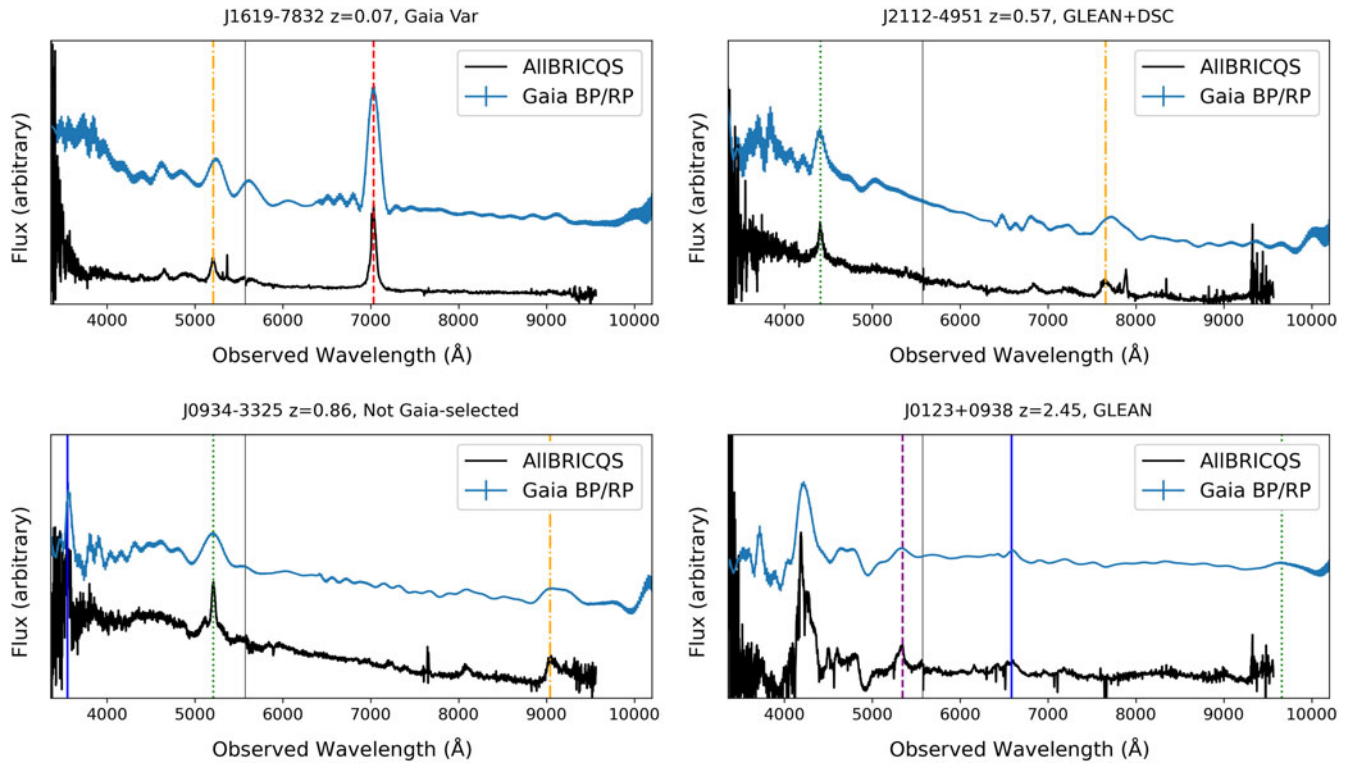[k] See https://gea.esac.esa.int/archive/documentation/GDR3/Data_analysis/chap_cu7var/sec_cu7var_agn/.

[l] See https://gea.esac.esa.int/archive/documentation/GDR3/Data_analysis/chap_cu7var/sec_cu7var_intro/ssec_cu7var_dataproducts.html.

[m] See Figure 11.13 from https://gea.esac.esa.int/archive/documentation/GDR3/Data_analysis/chap_cu8par/sec_cu8par_apsis/ssec_cu8par_apsis_dsc.html.

Figure 4. Flux versus wavelength for the $R \sim 3000$ spectrum of AllBRICQS (black line) and the *Gaia* low-resolution B_P/R_P spectral reconstruction (blue points with errorbars) for four example quasars. Top labels indicate the AllBRICQS redshift as well as the *Gaia* classifications (contained in GLEAN or other variability samples, and/or a DSC-labelled quasar). Vertical lines indicate the positions of various quasar emissions lines: Hα (red, dashed), Hβ (orange, dot-dashed), Mg II (green, dotted), C III (blue, solid), C IV (purple, dashed). The thin, black vertical line at 5575 Å indicates where the blue and red arms of the WiFeS spectrograph are spliced together. The *Gaia* spectra broaden and blend spectral features, which complicates the efforts to classify the sources and determine redshifts, let alone any more detailed analysis.

the luminous quasar at $z = 3.93$, was labelled as a star by the DSC with 99.98% probability.

In addition to the 116 quasars identified by the DSC, another 10 were flagged as quasars by the Outlier Analysis (OA) module, which uses self-organising maps (Kohonen 1982) to label sources with low DSC classification probability.

The challenges inherent in classifying quasars from *Gaia*'s low-resolution B_P/R_P spectroscopy are evident when comparing against our $R \sim 3000$ spectra from WiFeS (Figure 4). The blending of nearby emission lines, which can exhibit an intrinsic dispersion in relative fluxes, shifts the peak of the line emission, and the 'ringing' in the spectra reconstructed from the DR3 basis functions, both at the blue end and in regions around strong emission lines, often makes an assessment of the true underlying spectrum difficult. In terms of further analysis of the spectra, studies of absorption features (both broad and narrow) and emission line widths (e.g., for BH mass estimation) are only possible with higher resolving power than provided by the B_P/R_P spectra.

6.1. *Gaia-based redshift estimates*

Finally, we consider the performance of *Gaia*'s quasar classifier (QSOC; Delchambre et al. 2022) on the AllBRICQS objects. QSOC further analyses the DSC-labelled quasars (including those with quasar probabilities as low as 1%) to estimate redshifts from the B_P/R_P spectra. The method, trained on SDSS quasars, produced redshifts for 130 of the AllBRICQS quasars, including 96 quasars for which flags_qsoc $= 0$ (indicating reliable estimates). Among the latter, we find there to be one outlier, J2059-1632, a $z = 0.8$

quasar for which QSOC estimated $z = 3.146682 \pm 0.0089$ (mistaking Mg II for Lyα). Amongst the remaining 95 quasars, the QSOC redshift estimate is 0.001 too low in the mean, with a root-mean-square variation of less than 0.005. With a typical QSOC redshift uncertainty of 0.001, the differences are likely dominated by the limited redshift precision to which AllBRICQS aspires, and thus we confirm that QSOC is a highly effective tool for estimating quasar redshifts.

7. Discussion

The sources discovered in AllBRICQS are those which have eluded detection in the first 50+ yr of quasar searches, but many had already come under suspicion from other selection methods. In Section 6, we described the high degree of completeness for the *Gaia* quasar classification, which is remarkable given their exclusive reliance on *Gaia*'s optical dataset (astrometric, photometric, and low-resolution spectroscopic). Yet the existence of AllBRICQS quasars that escaped the *Gaia* criteria confirms the value of multi-wavelength approaches.

In addition to the *Gaia* variability and spectroscopic classifications, Table A.1 indicates the objects which were flagged as Primary or Secondary quasar candidates from the Ultraviolet Quasar Survey (UVQS; Monroe et al. 2016), which combined photometry from the *Galaxy Evolution Explorer* (*GALEX*; Martin et al. 2005) and *WISE* satellites. Apart from Galactic extinction, these UV/optical probes should provide the most complete samples of unobscured quasars at low to moderate redshift.

At higher energies, we anticipate the majority of the real quasars amongst the AllBRICQS candidates to be detected

by *SRG*/eROSITA (the *Spectrum-Roentgen-Gamma* satellite's extended ROentgen Survey with an Imaging Telescope Array; Predehl et al. 2021). In addition, a small number of AllBRICQS quasars are also known to be associated with quasar-like radio emission, but did not have a spectroscopically confirmed redshift.

Outliers from the AllBRICQS selection criteria (in either *Gaia* astrometry or *WISE* colours) could still be identified at other wavelengths, and many of those bright quasars may be observed as part of the Black Hole Mapper[n] (BHM) within SDSS-V (Kollmeier et al. 2017). Moreover, the BHM programme will greatly expand the samples at fainter optical magnitudes, particularly as SDSS extends its optical spectroscopy footprint to the Southern hemisphere.

Early large-area surveys for blue objects were limited to high Galactic latitude, with the Calán-Tololo Survey (Maza et al. 1988; Maza, Wischnjewsky, & Antezana 1996) and Hamburg Quasar Survey (Hagen et al. 1995; Hagen, Engels, & Reimers 1999) extending closest to the Galactic Plane ($|b| > 20°$) in the Southern and Northern hemispheres, respectively. Even DR1 of the UVQS, which focused on FUV-detected sources from *GALEX*, was incomplete in its coverage near the Plane because of the failure of the FUV detector prior to the relaxing of the satellite's initial safety constraints on overall count rates (see Bianchi 2014).

AllBRICQS is covering the sky down to $|b| > 10°$, but is still constrained from fully exploring behind the Galactic Plane because of source confusion arising from the limited spatial resolution of *WISE* (~6 arcsec in *W*1 and *W*2). Dedicated quasar searches within the Galactic Plane require alternative selection criteria to mitigate the effects of dust extinction, but have begun yielding significant samples (Im et al. 2007; Fu et al. 2021, 2022). Beyond photometric searches, additional low-latitude quasars may be uncovered thanks to the near-IR resolving power of the forthcoming *SPHEREx* satellite's all-sky spectrophotometric survey[o] (Crill et al. 2020).

AllBRICQS will complete observations of the target sample at declination $\delta < +20°$ with the ANU 2.3 m telescope at SSO. The intention for the Northern targets is to collect spectra at the Bohyunsan Optical Astronomy Observatory (BOAO) 1.8-m telescope and the Seoul National University Astronomical Observatory (SAO) 1.0-m telescope in South Korea, and the Yunnan Observatories (YNAO) Lijiang 2.4-m telescope at the Gaomeigu site near Lijiang, China. These observations will confirm classifications and determine redshifts, as well as enabling virial estimates of BH masses (see Cackett, Bentz, & Kara 2021, and references therein). They will also reveal unusual optical spectral properties and foreground absorbers, which may flag specific targets for detailed follow-up at other facilities.

In particular, the two bright quasars at $z > 2.5$—J0431-0838 at $z = 2.53$ with SMSS DR3 $i = 16.42$ ABmag, and J0529-4351 at $z = 3.93$ with $i = 16.07$ ABmag—may be appealing targets for the Sandage Test (Sandage 1962). With high-stability wavelength calibration and extremely large telescopes, it should soon be possible to directly detect the expansion of the Universe through the wavelength drift of intervening absorbers over time baselines of decades (Liske et al. 2008). These two AllBRICQS quasars, and subsequent discoveries at similar redshifts, would supplement the samples recently compiled by QUBRICS (QUasars as BRIght beacons for Cosmology in the Southern Hemisphere; Calderone et al. 2019; Boutsia et al. 2020) and ELQS (Extremely Luminous Quasar Survey; Schindler et al. 2017, 2019).

[n]See https://www.sdss5.org/mappers/black-hole-mapper/.
[o]See https://spherex.caltech.edu.

Finally, we note that a few AllBRICQS quasars were catalogued as AGNs by the Edinburgh-Cape (EC) Blue Object Survey, but because of the EC Survey's focus on hot, evolved stars in the Milky Way, the quasar spectra were not presented and no redshifts were recorded. We expect that many of the AllBRICQS candidates have been observed by groups looking for objects other than quasars, who seemingly had little incentive to publish those spectra—a situation which nearly held true for the case of J1144-4308 (Onken et al. 2022a). Yet even if AllBRICQS presents spectra of those objects in future papers, the historical datasets could hold enormous value for studies of variability properties and searches for changing-look AGNs (e.g., LaMassa et al. 2015), and we encourage readers to dust off their old datasets and publish their quasar spectra.

Data Availability. Photometry and spectroscopy from *Gaia* DR3 is publicly available. Photometric data from the other surveys utilised are publicly available. WiFeS spectroscopic data will be published upon completion of the AllBRICQS survey.

References

Abbott, T. M. C., et al. 2021, ApJS, 255, 20
Abdurro'uf, et al. 2022, ApJS, 259, 35
Bentz, M. C., et al. 2013, ApJ, 767, 149
Bianchi, L. 2014, Ap&SS, 354, 103
Boller, T., et al. 2016, A&A, 588, A103
Boutsia, K., et al. 2020, ApJS, 250, 26
Cackett, E. M., Bentz, M. C., & Kara, E. 2021, iScience, 24, 102557
Calderone, G., et al. 2019, ApJ, 887, 268
Carnerero, M. I., et al. 2022, arXiv e-prints, arXiv:2207.06849
Chambers, K. C., et al. 2016, arXiv e-prints, arXiv:1612.05560
Childress, M. J., Vogt, F. P. A., Nielsen, J., & Sharp, R. G. 2014, Ap&SS, 349, 617
Crill, B. P., et al. 2020, in Society of Photo-Optical Instrumentation Engineers (SPIE) Conference Series, Vol. 11443, Society of Photo-Optical Instrumentation Engineers (SPIE) Conference Series, 114430I
De Angeli, F., et al. 2022, arXiv e-prints, arXiv:2206.06143
Delchambre, L., et al. 2022, arXiv e-prints, arXiv:2206.06710
Desai, S., et al. 2012, ApJ, 757, 83
Dopita, M., et al. 2007, Ap&SS, 310, 255
Dopita, M., et al. 2010, Ap&SS, 327, 245
Drlica-Wagner, A., et al. 2022, ApJS, 261, 38
Fitzpatrick, E. L., Massa, D., Gordon, K. D., Bohlin, R., & Clayton, G. C. 2019, ApJ, 886, 108
Flaugher, B., et al. 2015, AJ, 150, 150
Flesch, E. W. 2021, arXiv e-prints, arXiv:2105.12985
Fu, Y., et al. 2022, ApJS, 261, 32
Fu, Y., et al. 2021, ApJS, 254, 6
Gaia Collaboration. 2016, A&A, 595, A1
Gaia Collaboration. 2021, A&A, 649, A1
Gaia Collaboration. 2022, arXiv e-prints, arXiv:2206.05681
Geller, M. J., et al. 2016, ApJS, 224, 11
Gordon, K. 2021, karllark/dust_extinction: interstellar dust extinction curves, Zenodo
Gravity Collaboration, et al. 2021a, A&A, 654, A85
Gravity Collaboration, et al. 2021b, A&A, 648, A117
Gravity Collaboration, et al. 2020, A&A, 643, A154
Gravity Collaboration, et al. 2018, Natur, 563, 657
Hagen, H. J., Engels, D., & Reimers, D. 1999, A&AS, 134, 483
Hagen, H. J., Groote, D., Engels, D., & Reimers, D. 1995, A&AS, 111, 195
Hale, C. L., et al. 2021, PASA, 38, e058
Hinton, S. 2016, MARZ: Redshifting Program, Astrophysics Source Code Library, record ascl:1605.001
Hinton, S. R., Davis, T. M., Lidman, C., Glazebrook, K., & Lewis, G. F. 2016, A&C, 15, 61
Im, M., et al. 2007, ApJ, 664, 64
Izumi, T., et al. 2020, ApJ, 898, 61
Kilkenny, D., et al. 2016, MNRAS, 459, 4343
Klemola, A. R., Jones, B. F., & Hanson, R. B. 1987, AJ, 94, 501
Kohonen, T. 1982, BC, 43, 59
Kollmeier, J. A., et al. 2017, arXiv e-prints, arXiv:1711.03234
LaMassa, S. M., et al. 2015, ApJ, 800, 144
Lemon, C., et al. 2022, arXiv e-prints, arXiv:2206.07714
Lemon, C. A., Auger, M. W., & McMahon, R. G. 2019, MNRAS, 483, 4242
Liao, S., 2021, PASP, 133, 094501
Liske, J., et al. 2008, MNRAS, 386, 1192
Mainzer, A., et al. 2014, ApJ, 792, 30
Marocco, F., et al. 2021, ApJS, 253, 8
Martin, D. C., et al. 2005, ApJ, 619, L1
Maza, J., Ruiz, M. T., Gonzalez, L. E., & Wischnjewski, M. 1988, in Astronomical Society of the Pacific Conference Series, Vol. 1, Progress and Opportunities in Southern Hemisphere Optical Astronomy. The CTIO 25th Anniversary Symposium, ed. V. M. Blanco, & M. M. Phillips, 410
Maza, J., Wischnjewsky, M., & Antezana, R. 1996, RMxAA, 32, 35
McConnell, D., et al. 2020, PASA, 37, e048
McQuinn, M. 2016, ARA&A, 54, 313
Monroe, T. R., et al. 2016, AJ, 152, 25
Montegriffo, P., et al. 2022, arXiv e-prints, arXiv:2206.06205
Nidever, D. L., et al. 2021, AJ, 161, 192
Onken, C. A., et al. 2020, MNRAS, 496, 2309
Onken, C. A., et al. 2022a, arXiv e-prints, arXiv:2206.04204
Onken, C. A., et al. 2019, PASA, 36, e033
Onken, C. A., et al. 2022b, MNRAS, 511, 572
Predehl, P., et al. 2021, A&A, 647, A1
Rakshit, S., Stalin, C. S., & Kotilainen, J. 2020, ApJS, 249, 17
Richards, G. T., et al. 2002, AJ, 123, 2945
Riello, M., et al. 2021, A&A, 649, A3

Runnoe, J. C., Brotherton, M. S., & Shang, Z. 2012a, MNRAS, 427, 1800
Runnoe, J. C., Brotherton, M. S., & Shang, Z. 2012b, MNRAS, 422, 478
Sandage, A. 1962, ApJ, 136, 319
Schindler, J.-T., et al. 2019, ApJ, 871, 258
Schindler, J.-T., et al. 2017, ApJ, 851, 13
Schlafly, E. F. & Finkbeiner, D. P. 2011, ApJ, 737, 103
Schlegel, D. J., Finkbeiner, D. P., & Davis, M. 1998, ApJ, 500, 525
Shu, Y., et al. 2019, MNRAS, 489, 4741
Souchay, J., et al. 2022, A&A, 660, A16
Stobie, R. S., et al. 1997, MNRAS, 287, 848
Tumlinson, J., Peeples, M. S., &Werk, J. K. 2017, ARA&A, 55, 389
Valdes, F., Gruendl, R., & DES Project. 2014, in Astronomical Society of the Pacific Conference Series, Vol. 485, Astronomical Data Analysis Software and Systems XXIII, ed. N. Manset, & P. Forshay, 379

Waters, C. Z., et al. 2020, ApJS, 251, 4
Wisotzki, L., et al. 2000, A&A, 358, 77
Wolf, C., et al. 2018a, PASA, 35, e024
Wolf, C., et al. 2020, MNRAS, 491, 1970
Wolf, C., et al. 2018b, PASA, 35, e010
Wright, E. L., et al. 2010, AJ, 140, 1868
Wu, Q.-Q., et al. 2022, FrASS, 9, 822768
York, D. G., et al. 2000, AJ, 120, 1579

Appendix A. AllBRICQS Confirmed Quasars

We list the properties of the confirmed AllBRICQS quasars in Table A.1, arranged in order of ascending RA. The $W1 - W2$ colour is taken from the more accurate of CatWISE2020 (Marocco

Table A.1. Confirmed AllBRICQS quasars.

Name	*Gaia* DR3 SOURCE_ID	RA (J2000)	Dec (J2000)	B_P	R_P	$W1 - W2$	Redshift	UVQS	*Gaia*	Notes
		deg	deg	mag	mag	mag				
J0000-7524	4685240533123833088	0.1563	−75.4118	16.46	15.75	1.05	0.23	1	GD	
J0006-6457	4900255628276737792	1.5663	−64.9616	16.51	15.81	1.19	1.724	–	GD	
J0010-6959	4702951122826363904	2.6084	−69.9870	15.64	15.12	1.19	0.423	–	GD	
J0010-0702	2441707363251993216	2.6482	−7.0423	16.48	16.05	0.99	0.207	2	GD	
J0014-2235	2361107938255080832	3.6834	−22.5896	16.39	15.85	1.40	1.44	1	GD	
J0028-4054	4993849326503326720	7.2018	−40.9038	16.20	15.71	1.04	0.219	–	GD	
J0035-7820	4635525182864394368	8.9961	−78.3403	16.43	15.84	1.32	0.96	–	GD	1
J0056+1141	2582790132617218048	14.2319	11.6984	17.32	15.99	0.98	1.65	–	--	2
J0117-1712	2355371511215136384	19.4378	−17.2117	16.39	15.83	0.76	0.68	–	GD	
J0123+0938	2579205655991234048	20.8272	9.6372	16.70	15.73	0.68	2.45	–	G–	
J0140-0653	2479251287293182592	25.1431	−6.8958	16.13	15.50	0.98	0.2	2	GD	
J0141-1607	2452322735700697600	25.3660	−16.1270	16.79	15.93	1.18	0.66	–	GD	
J0146-2608	5025447435259941376	26.6884	−26.1460	16.58	15.92	1.12	0.614	–	–D	
J0154-5559	4719544299477963520	28.6425	−55.9846	15.57	14.94	1.17	1.6	–	GD	
J0159-3205	5018050883101214848	29.8456	−32.0894	16.76	16.00	1.48	1.056	–	vD	
J0201+1134	2574519674872605184	30.4064	11.5759	16.58	15.83	1.01	0.203	1	GD	
J0207-2354	5121675902648838656	31.9490	−23.9029	14.90	14.29	0.92	0.076	–	GD	3
J0210-5321	4743906728370668288	32.6818	−53.3561	16.78	15.95	1.41	1.52	–	v–	
J0219+1925	87024356769335808	34.9021	19.4266	16.27	15.50	1.19	0.824	–	G–	
J0220-2519	5119524364551391872	35.2302	−25.3242	16.54	15.93	1.24	2.173	–	GD	
J0241-1719	5132542547864397056	40.4892	−17.3173	15.98	15.51	1.00	0.187	2	GD	
J0245-8035	4619847113421226240	41.4709	−80.5927	16.19	15.70	1.32	0.927	1	GD	
J0252-2650	5072673246379455104	43.1902	−26.8473	16.44	15.87	1.17	0.83	–	GD	
J0311-4655	4750861929689855360	47.9983	−46.9300	16.90	15.67	1.12	0.5546	–	G–	
J0315-7434	4639775757378274944	48.9038	−74.5695	16.41	15.96	1.23	0.691	–	GD	
J0316-0919	5166622494882955520	49.2104	−9.3253	16.42	15.67	1.42	0.287	–	GD	
J0327-7224	4642275673158740224	51.7594	−72.4010	16.06	15.41	0.86	0.126	2	GD	1
J0328-6225	4674156528202556160	52.0129	−62.4254	16.15	15.56	1.06	0.18	–	GD	1
J0343-1711	5108385074813114496	55.8885	−17.1857	15.64	15.07	1.28	0.66	–	GD	1
J0400-2257	5090217427573688192	60.1855	−22.9534	16.33	15.58	0.95	0.163	2	GD	
J0405-2410	5089142453095475840	61.4342	−24.1808	16.45	15.94	1.46	1.26	–	GD	
J0425-4410	4839258610114187264	66.3719	−44.1693	15.26	14.85	1.09	0.39	–	–D	1
J0427-1412	3175855537725581952	66.7904	−14.2024	16.59	15.98	1.12	0.388	–	GD	1
J0431-0838	3197674349547449856	67.7730	−8.6407	17.07	15.98	0.96	2.53	–	G–	

Table A.1. Continued.

Name	*Gaia* DR3 source_id	RA (J2000)	Dec (J2000)	B_P	R_P	$W1 - W2$	Redshift	UVQS	*Gaia*	Notes
		deg	deg	mag	mag	mag				
J0433-0641	3198628966157590784	68.3834	−6.6968	16.49	16.20	1.28	0.81	–	GD	
J0500-6322	4665166852415732352	75.0027	−63.3771	15.96	15.52	1.23	1.18	–	GD	
J0502-2002	2975142095258671744	75.5014	−20.0368	16.24	15.64	1.16	0.375	–	GD	
J0502-6227	4664566278549403392	75.7110	−62.4613	16.24	15.80	1.11	0.382	2	GD	1
J0504+0055	3228636356466440320	76.2366	0.9272	15.90	15.06	0.88	2.34	–	G−	
J0513-3320	4826131231553088896	78.3498	−33.3358	16.53	15.81	1.16	0.419	–	GD	
J0514-1618	2983155095483011584	78.6401	−16.3106	16.54	15.87	1.23	0.2272	–	GD	
J0529-4351	4805630493655815040	82.3159	−43.8645	16.91	15.69	0.38	3.93	–	v−	
J0530+0042	3221158234288319744	82.6800	0.7118	16.28	15.70	1.15	0.7	–	GD	
J0533-1434	2984416785075086336	83.2543	−14.5704	16.30	15.60	1.00	0.139	2	GD	
J0546-4630	4795962449256424448	86.6186	−46.5021	16.43	15.90	1.08	0.279	2	GD	
J0555-5100	4792646051605064832	88.8761	−51.0048	16.43	15.88	1.02	0.263	–	vD	
J0600-4105	2882337747595526528	90.0612	−41.0911	16.04	15.48	1.40	1.19	–	GD	
J0603-3110	2890998291450368896	90.8093	−31.1790	16.37	15.94	1.15	0.726	–	GD	
J0624-6324	5477304692317531392	96.1551	−63.4118	15.94	15.38	1.19	0.576	–	GD	
J0624-2545	2900007414852025088	96.2033	−25.7659	15.16	14.46	0.83	0.863	–	G−	
J0634-6945	5278908676764365824	98.7319	−69.7589	15.99	15.36	1.34	1.37	–	−−	
J0639-2653	2919897167882522496	99.9759	−26.8965	16.26	15.55	1.15	0.705	–	G−	
J0712-5659	5486909991537522688	108.0864	−56.9940	15.49	15.00	1.36	0.907	–	GD	
J0715-4951	5505302725127883136	108.7923	−49.8524	15.04	14.05	0.80	0.1156	–	v−	
J0749+0203	3088492604393071488	117.4535	2.0600	15.90	15.44	1.13	0.374	–	GD	
J0818-7933	5208653628959060608	124.5859	−79.5603	15.95	15.34	1.43	1.29	–	GD	
J0833-0628	5754948798717254144	128.4389	−6.4800	16.25	15.77	1.36	1.2	–	GD	4
J0835-0833	5753659140297301760	128.8037	−8.5636	15.99	15.63	1.08	0.585	–	GD	
J0854-0718	5756861914589220736	133.6467	−7.3104	16.24	15.53	1.03	1.14	–	GD	
J0907-2000	5680217153745527936	136.9000	−20.0005	16.32	15.83	1.16	0.57	1	GD	5
J0930-7528	5215913601159378944	142.6517	−75.4817	16.14	15.50	1.10	0.35	–	GD	
J0934-3325	5438016461800707712	143.6061	−33.4233	16.39	15.73	1.12	0.86	–	−−	
J1037-2223	5474848486419684096	159.4465	−22.3887	16.13	15.70	1.30	0.96	–	GD	1
J1040-3324	5444798279580321536	160.1045	−33.4127	16.16	15.55	1.21	1.04	–	GD	
J1048-3401	5449737908584117376	162.1377	−34.0227	16.01	15.44	1.21	1.19	–	G−	
J1049-3001	5454621252040188672	162.4913	−30.0177	16.50	15.98	1.14	1.44	–	GD	
J1120-2939	3482845025356707584	170.2026	−29.6608	16.49	16.04	1.17	0.65	1	GD	1
J1128-7435	5225252406250984448	172.0981	−74.5935	16.36	15.21	1.28	1.48	–	−−	
J1205+0845	3905774372003183360	181.3565	8.7508	16.36	15.81	0.92	0.935	–	GD	
J1215-3221	3469391607236907392	183.8098	−32.3505	16.50	15.85	0.93	0.1727	2	vD	
J1227-4133	6146727950157752320	186.9019	−41.5519	16.54	15.86	1.29	0.99	–	GD	
J1249-3545	6155619047856315776	192.3628	−35.7587	16.77	15.94	1.07	0.39	–	−−	
J1252-3928	6152529110943401216	193.1630	−39.4697	16.59	15.69	0.91	0.2345	–	GD	
J1304-2318	3504140465345674624	196.2204	−23.3147	15.40	14.60	1.10	0.3785	–	GD	
J1333-2249	6194977063004413312	203.3060	−22.8319	16.70	15.55	1.12	0.8	–	G−	
J1345-4847	6094779942759884416	206.3290	−48.7969	16.62	15.63	1.32	0.737	–	G−	
J1350-2924	6176765302157977856	207.6995	−29.4011	16.54	15.97	1.32	1.09	–	vD	
J1357-3352	6170515643706741632	209.3862	−33.8703	16.34	15.88	1.32	0.99	–	GD	
J1409-3704	6120955535042511744	212.4075	−37.0801	16.39	15.77	1.38	1.05	–	GD	
J1410-3824	6117445893933200128	212.5764	−38.4076	16.91	16.30	1.04	1.65	–	−D	6
J1416-1330	6302999235710077312	214.1154	−13.5025	16.91	16.29	1.29	1.13	–	GD	6

Table A.1. Continued.

Name	*Gaia* DR3 SOURCE_ID	RA (J2000) deg	Dec (J2000) deg	B_P mag	R_P mag	$W1 - W2$ mag	Redshift	UVQS	*Gaia*	Notes
J1419-7303	5797309644547609472	214.8014	−73.0636	16.37	15.68	1.04	0.32	−	G−	
J1422-2453	6272600006945299072	215.5091	−24.8835	16.75	15.83	1.25	1.35	−	GD	
J1424-3833	6116655241990813056	216.2170	−38.5578	16.40	15.80	1.24	0.92	−	vD	
J1427-4251	6102649972113553024	216.8860	−42.8549	15.49	14.79	0.92	0.25	−	GD	
J1455-4744	5905051652260501248	223.8729	−47.7491	16.17	15.30	0.86	0.202	−	GD	
J1458-1621	6306813128014139776	224.7167	−16.3514	16.95	15.89	1.23	0.587	−	G−	
J1459-7714	5791742855834137472	224.7994	−77.2455	15.98	15.53	1.21	0.648	−	GD	
J1501-1053	6313702809608036736	225.2787	−10.8903	16.71	16.12	1.13	0.72	−	vD	6
J1509-3950	6005386039652374784	227.3979	−39.8405	16.98	16.50	1.32	0.91	−	−D	6
J1518-1736	6258932798238246912	229.5049	−17.6045	16.28	15.36	1.13	0.68	−	GD	
J1518-2308	6251379947930795520	229.5082	−23.1337	16.47	15.95	1.03	0.93	−	GD	
J1527-7828	5779460245798329984	231.7948	−78.4740	16.03	15.46	1.25	0.95	−	−D	
J1538-4004	6002928699894118656	234.6418	−40.0758	16.62	15.89	1.02	0.1518	−	−D	
J1544-2016	6241880304902964352	236.1084	−20.2762	15.25	14.43	1.06	0.23	−	GD	
J1546-8422	5768119230033216128	236.6550	−84.3732	16.57	15.97	1.15	0.374	−	GD	
J1547-1449	6263682211733086720	236.7656	−14.8272	16.49	15.76	1.25	1.32	−	GD	
J1554-3209	6039417264563751808	238.6295	−32.1637	15.69	14.79	1.17	0.278	−	GD	
J1559-6732	5822042647531326208	239.9957	−67.5439	15.95	15.43	1.17	0.629	−	GD	
J1601-7202	5818662336458884224	240.4902	−72.0431	15.66	14.87	0.96	0.1045	−	GD	
J1607-0740	4348755065537927296	241.8802	−7.6732	16.76	15.78	0.94	0.2086	−	GD	
J1612-6958	5819359564272623104	243.0770	−69.9812	16.08	15.47	1.21	1.37	−	−D	
J1618-3059	6037522256277200256	244.5586	−30.9907	17.11	15.95	1.03	0.088	−	−−	
J1618-1424	4329648611456994176	244.6891	−14.4070	16.67	15.71	0.98	0.207	−	GD	
J1619-7832	5778852799983279744	244.7576	−78.5437	14.97	14.10	0.89	0.072	1	v−	
J1622+1400	4463914614888824064	245.5325	14.0136	16.38	15.83	0.92	0.93	−	GD	
J1654+0742	4442283510319657216	253.5757	7.7012	16.68	15.92	1.12	0.327	−	GD	
J1705+1354	4544604509076327936	256.4004	13.9051	16.74	15.79	1.45	1.3	−	v−	
J1720+1115	4540223539356310784	260.0047	11.2502	16.31	15.55	0.89	0.184	1	GD	
J1726+0128	4375126680125658880	261.5279	1.4796	16.68	15.75	1.49	1.6	−	−−	
J1728+1954	4554115250297917952	262.0982	19.9007	16.44	15.95	1.24	0.94	−	GD	
J1738+0042	4375310569150345216	264.7142	0.7106	16.65	15.81	1.08	0.212	−	−D	
J1817-4144	6724670225684293248	274.4713	−41.7349	16.30	15.69	0.89	0.1978	−	−D	
J1904-1706	4088315532990245376	286.0108	−17.1147	16.12	15.18	1.01	0.1995	−	G−	
J1904-5640	6642902913158050816	286.0246	−56.6740	16.46	15.59	1.38	0.777	−	G−	
J1905-2639	6763933442298679040	286.3691	−26.6542	15.99	14.97	1.07	0.121	−	G−	
J1910-4809	6661621033470406656	287.7193	−48.1629	16.47	15.98	1.16	0.7677	−	GD	
J1916-1842	4084303552485486336	289.2401	−18.7078	16.91	15.92	0.99	0.155	−	−−	
J1933-2129	6772236331332883840	293.3253	−21.4843	16.20	15.66	1.11	0.855	−	GD	
J2000-4658	6671681324343864832	300.0483	−46.9695	16.06	15.15	1.19	0.555	−	G−	1
J2006+1032	4300542923775269248	301.6039	10.5496	16.30	15.34	0.82	1.85	−	G−	
J2007+1235	1803066685791351168	301.9853	12.5882	16.20	15.62	1.12	0.4	−	GD	
J2034-0405	4218657791715405952	308.5555	−4.0914	16.02	15.26	0.87	0.0995	2	G−	
J2048-6923	6376205952542312192	312.0243	−69.3988	16.67	15.96	1.08	0.328	1	GD	
J2050-2530	6805397468883982464	312.5629	−25.5098	16.55	15.95	1.25	0.883	−	GD	
J2055-4014	6773780084311817472	313.9932	−40.2429	16.50	15.25	0.66	1.86	−	−−	
J2058-1452	6886716902195844352	314.5257	−14.8761	15.86	15.27	0.92	0.135	1	GD	
J2059-1632	6883214987725624320	314.8057	−16.5483	16.44	16.00	1.19	0.8	−	GD	
J2101+1350	1758570133100303872	315.2916	13.8339	16.97	15.93	0.88	1.419	−	v−	

Table A.1. Continued.

Name	*Gaia* DR3 SOURCE_ID	RA (J2000)	Dec (J2000)	B_P	R_P	$W1 - W2$	Redshift	UVQS	*Gaia*	Notes
		deg	deg	mag	mag	mag				
J2101-3834	6774357224839696256	315.4377	−38.5680	16.11	15.68	1.32	0.767	−	GD	1
J2102-7733	6368144814324065536	315.6306	−77.5598	16.21	15.55	1.40	0.89	1	G−	1
J2107-6525	6449304925828127104	316.8300	−65.4219	16.43	16.02	1.11	0.567	1	GD	
J2111-4949	6478751805723581952	317.9159	−49.8229	16.52	15.96	0.92	0.336	1	GD	
J2112-4951	6478748678987384448	318.0231	−49.8604	16.40	16.06	1.22	0.575	1	GD	
J2113-5840	6453491488148613760	318.4068	−58.6791	15.87	15.44	0.85	0.99	−	GD	
J2114+1637	1784845196828559360	318.7141	16.6293	16.40	15.61	1.12	1.265	−	v−	
J2116-5931	6453194443914776320	319.0123	−59.5296	16.62	15.93	1.05	1.75	−	−D	
J2119-0929	6895824775484040832	319.8336	−9.4970	16.18	15.37	0.85	1.21	−	G−	
J2126-4529	6576106447897533440	321.7254	−45.4994	16.99	15.78	1.11	0.167	−	G−	
J2128-7059	6372260702960045184	322.2374	−70.9871	15.87	15.50	1.05	0.477	−	GD	1
J2135+0858	1741107281406118656	323.7702	8.9668	16.43	15.94	0.24	0.25	−	GD	
J2149+1827	1774065898363122560	327.3104	18.4642	16.67	15.98	0.86	0.878	−	G−	
J2156-2400	6813438021321493120	329.2228	−24.0157	16.51	15.42	1.31	0.87	−	G−	
J2207-1654	6826143908972604672	331.9871	−16.9110	16.88	15.94	0.92	0.1288	−	GD	
J2234-6757	6385868911699682304	338.6292	−67.9561	16.48	15.55	1.00	0.365	−	G−	
J2242-1316	2598238648944896640	340.7390	−13.2830	15.93	15.37	1.05	0.274	−	GD	7
J2248-2446	6623320817223115776	342.1243	−24.7827	16.65	15.94	1.38	1.62	−	GD	
J2306-2604	2382576796140530432	346.5987	−26.0782	16.37	16.01	1.36	1.04	−	GD	
J2316-1941	2392891623957984768	349.1658	−19.6871	16.49	16.08	1.25	0.99	1	GD	
J2320-0524	2633514757239529728	350.1815	−5.4126	16.03	15.47	1.00	1.368	−	GD	
J2321-1521	2408315676151838080	350.3087	−15.3584	16.44	15.99	1.18	0.665	−	vD	
J2324-4250	6535888953956911232	351.1461	−42.8426	16.51	15.98	1.20	0.97	−	GD	
J2329-2133	2388531854195433344	352.4782	−21.5658	15.81	15.28	1.12	0.32	2	GD	7
J2331-6642	6389695349603211008	352.8306	−66.7006	16.50	15.73	0.96	0.274	1	GD	
J2343-4519	6531466172730996096	355.8729	−45.3279	15.97	15.37	1.23	0.813	−	GD	
J2344-1121	2432988884582722560	356.0001	−11.3665	16.47	16.10	1.25	0.65	1	GD	

Position information from Gaia DR3.
1. Known quasar from Edinburgh-Cape Blue Object Survey, but redshift not recorded.
2. Known quasar with $z = 1.656$ from Geller et al. (2016), but no spectrum presented. Data available from CfA Optical/Infrared Science Archive.
3. Known quasar with $z = 0.076$ from Izumi et al. (2020), but no spectrum presented.
4. Known quasar with $z = 1.201$ recently discovered by Fu et al. (2022).
5. UVQS DR1 source catalogued as $z = 1.279$ having z_qual=0 ("no estimate possible").
6. Extended selection criteria: $B_P > 16.5$ and $R_P > 16$ mag.
7. Reported as star in the Lick Northern Proper Motion survey (Klemola et al. 1987).

et al. 2021) and AllWISE.[p] The 'UVQS' column indicates whether the source was a primary ('1') or secondary ('2') candidate in the FUV-selected sample from UVQS DR1 (Monroe et al. 2016). The 'Gaia' column is a two-element code indicating (1) whether the source is included in the *Gaia* DR3 variabLE AgN sample ('G'; Carnerero et al. 2022), or only in another *Gaia* DR3 variability table [q] ('v'); and (2) whether the source has classlabel_dsc='quasar' according to the *Gaia* Discrete Source Classifier ('D'). Sources not meeting one criteria or the other (or both) are indicated with '−'.

[p]See https://wise2.ipac.caltech.edu/docs/release/allwise/expsup/index.html.
[q]See https://gea.esac.esa.int/archive/documentation/GDR3/Data_analysis/chap_cu7var/sec_cu7var_intro/ssec_cu7var_dataproducts.html.

In the table notes, we indicate two sources of known redshift for which optical spectra had not been previously published; 13 sources identified as quasars from the Edinburgh-Cape Blue Object Survey (Stobie et al. 1997; Kilkenny et al. 2016), but without published redshifts (intentionally retained in the AllBRICQS target list); one source at $b = +19.3°$ discovered by Fu et al. (2022) during preparation of this manuscript; one source with a low-quality redshift estimate from UVQS DR1, which we revise; and two quasars mistakenly catalogued as stars in the Lick Northern Proper Motion survey (Klemola, Jones, & Hanson 1987, with one also in Milliquas as a star with radio detection). We also flag four quasars taken from a magnitude bin 0.5 mag fainter than the nominal AllBRICQS limits.

Appendix B. Gallery of AllBRICQS Quasar Spectra

We present the WiFeS spectra for the AllBRICQS quasars in Figures B.1–B.13, arranged in order of ascending redshift.
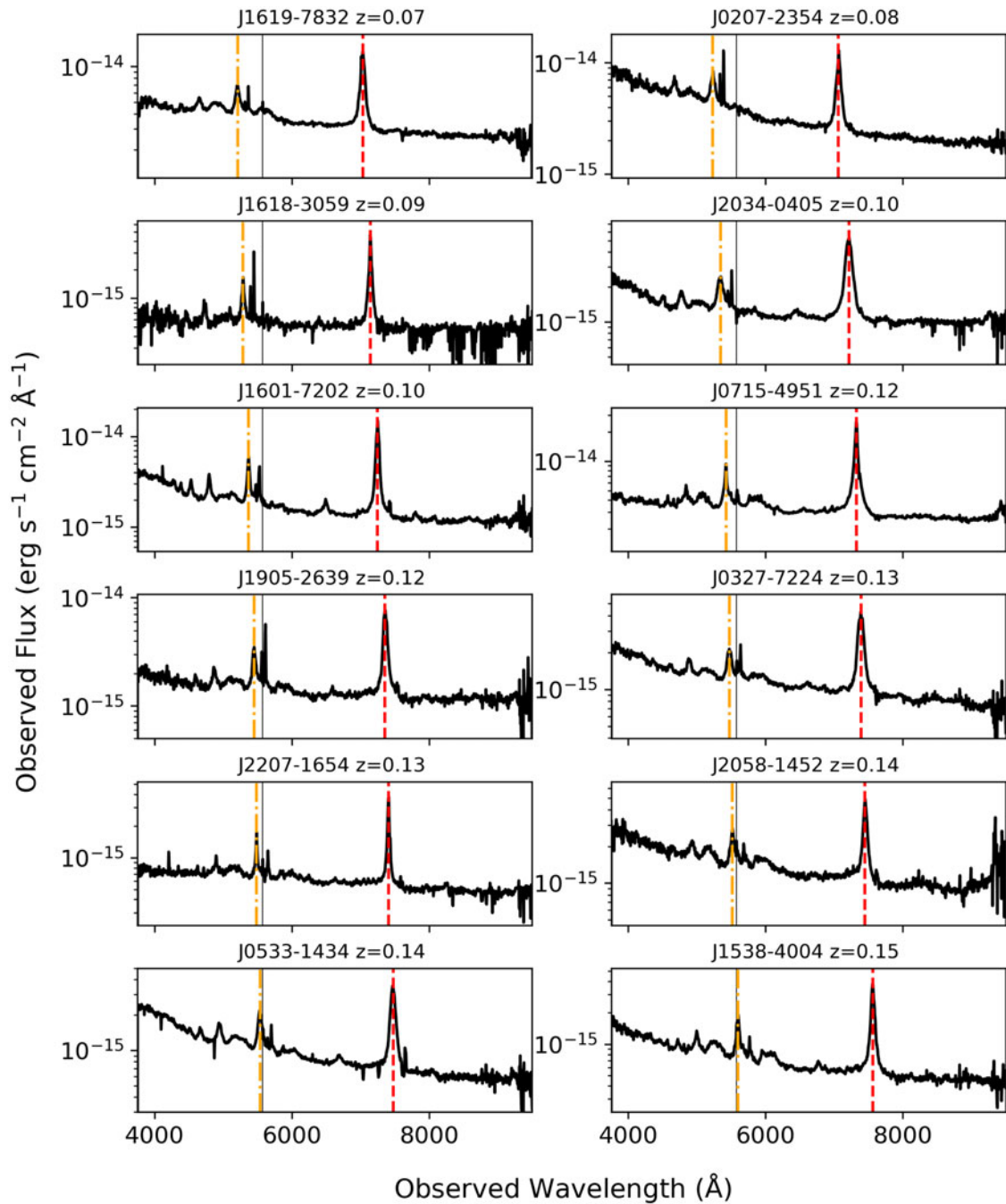
Figure B.1. WiFeS spectra of the AllBRICQS sample, shown with increasing redshift. The *y*-axis hows the flux on a logarithmic scale, normalised using Gaia DR3 photometry. Vertical lines indicate the positions of various quasar emissions lines: Hα (red, dashed), Hβ (orange, dot-dashed), Mg II (green, dotted), C III] (blue, solid), C IV (purple, dashed). The thin, black vertical line at 5575 Å indicates where the blue and red arms of the spectrograph are spliced together.

Figure B.2. As in Figure B.1.

Figure B.3. As in Figure B.1.

Figure B.4. As in Figure B.1.

Figure B.5. As in Figure B.1.

Figure B.6. As in Figure B.1.

Figure B.7. As in Figure B.1.

Figure B.8. As in Figure B.1.

Figure B.9. As in Figure B.1.

Figure B.10. As in Figure B.1.
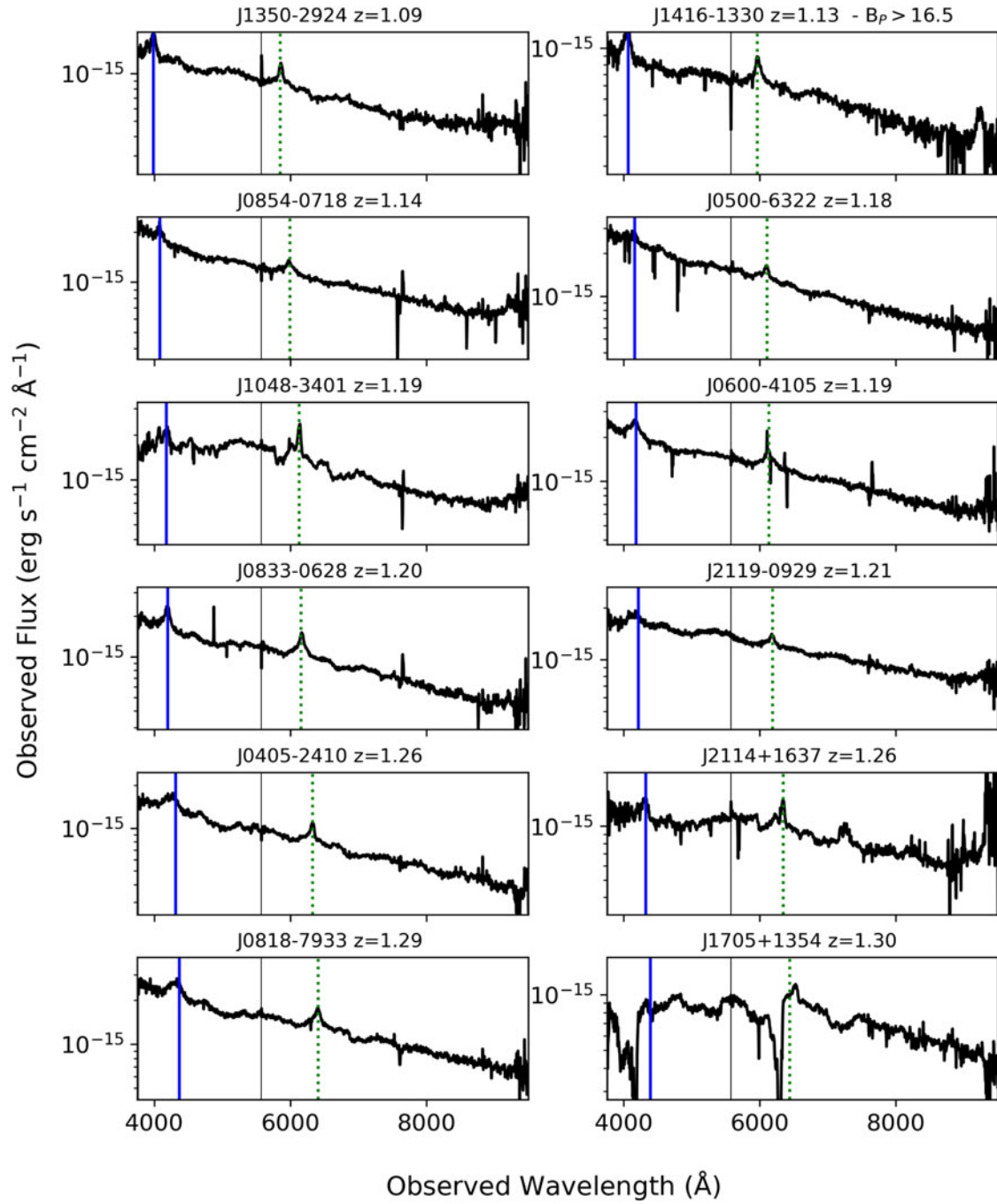
Figure B.11. As in Figure B.1.
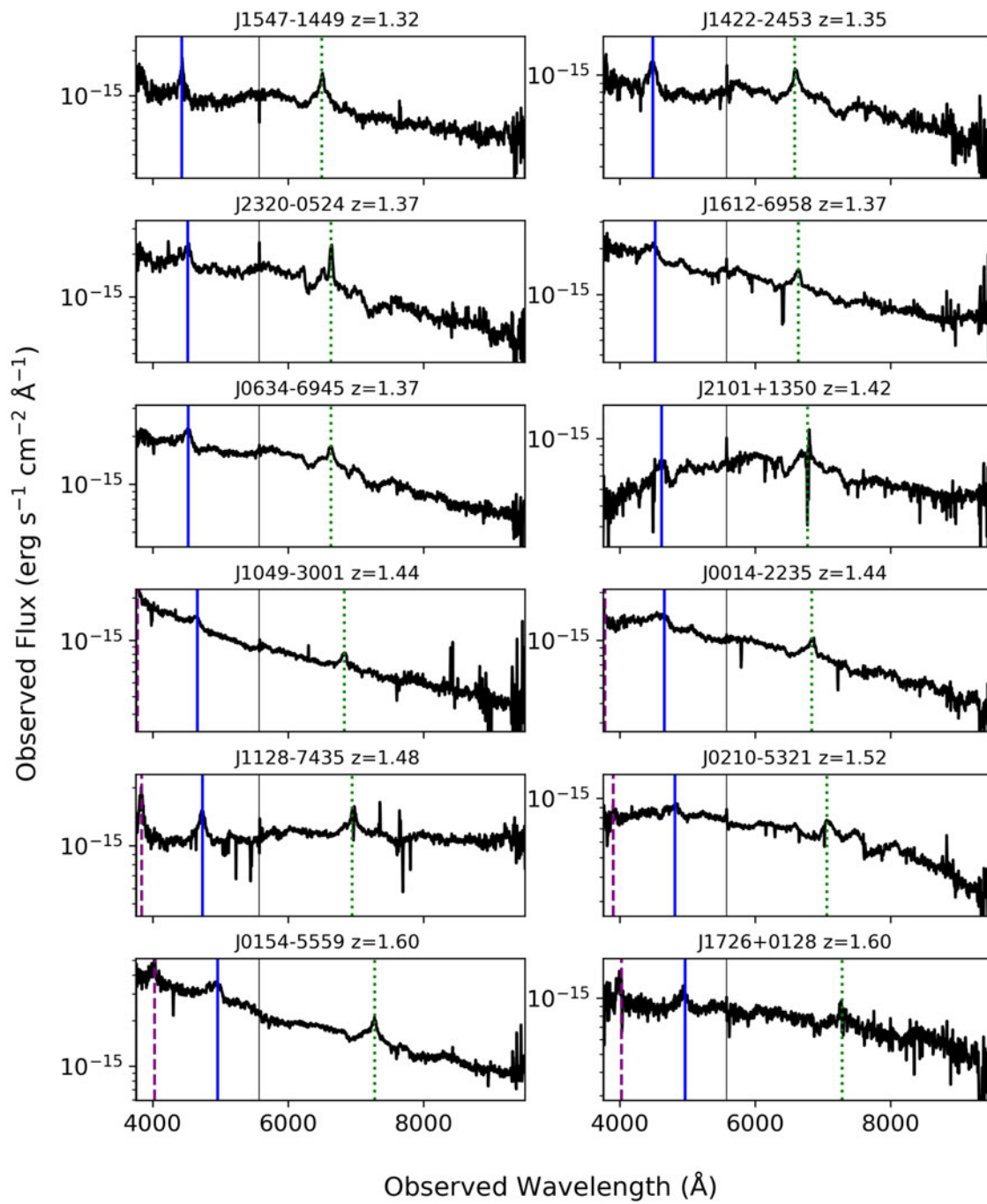
Figure B.12. As in Figure B.1.
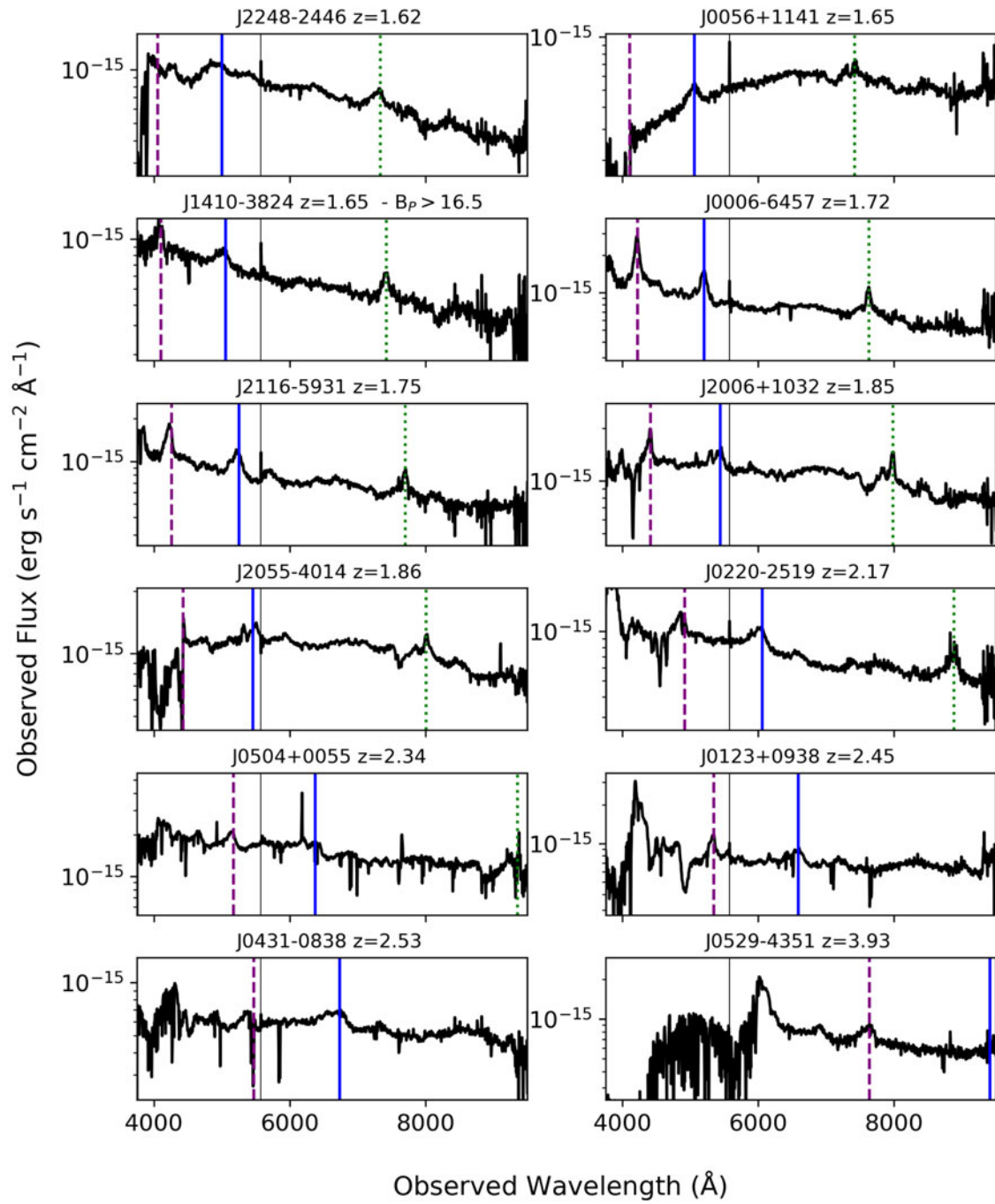
Figure B.13. As in Figure B.1.

Appendix C. Unclassified sources observed in AllBRICQS

Table C.1 presents the sources which remain unclassified. Column
definitions as in Appendix A. We also present the WiFeS spectra
for the unclassified sources in Figure C.1.

Table C.1. Unidentified AllBRICQS sources.

Name	*Gaia* DR3 SOURCE_ID	RA (J2000)	Dec (J2000)	B_P	R_P	$W1 - W2$	UVQS	*Gaia*	Notes
		deg	deg	mag	mag	mag			
J0304-6020	4723537966228181376	46.1515	−60.3482	15.62	15.11	1.21	–	GD	
J1728+0916	4490941985090542720	262.2476	9.2697	16.30	15.68	1.25	–	GD	
J2309-1512	2410041905112464256	347.4918	−15.2019	16.21	15.18	1.28	–	G–	Possible $z = 0.54$
J2331-0836	2437563029048114176	352.8658	−8.6121	16.47	16.12	1.12	–	GD	Possible $z = 0.66$

Position information from Gaia DR3
Column definitions as in Table A.1.
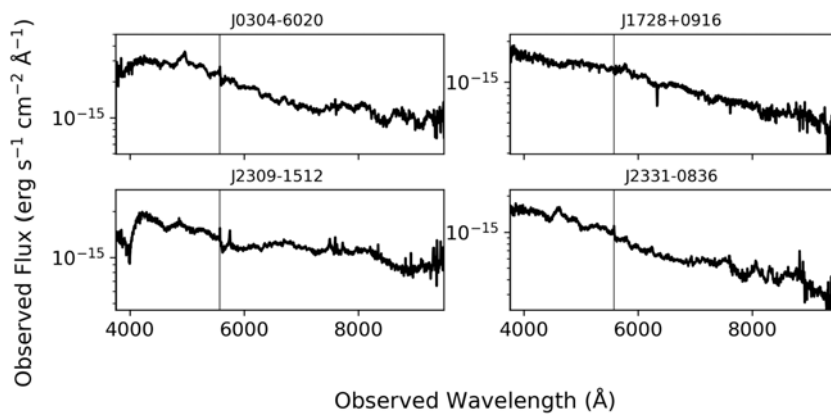
Figure C.1. WiFeS spectra of the unclassified sources observed in AllBRICQS. The *y*-axis shows the flux on a logarithmic scale, normalised using their Gaia DR3 photometry. The
thin, black vertical line at 5575 Å indicates where the blue and red arms of the spectrograph are spliced together.

Appendix D. Stars observed in AllBRICQS
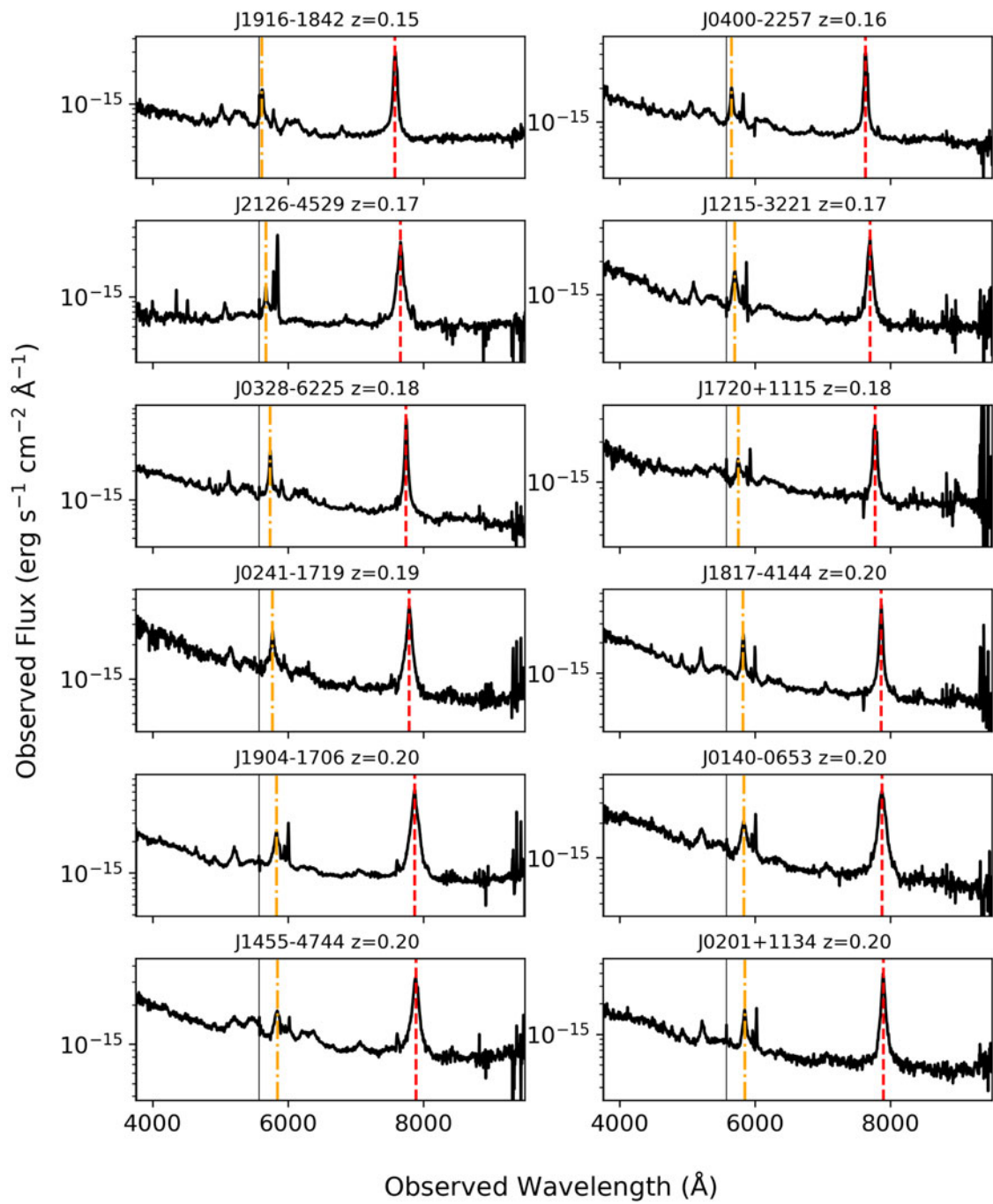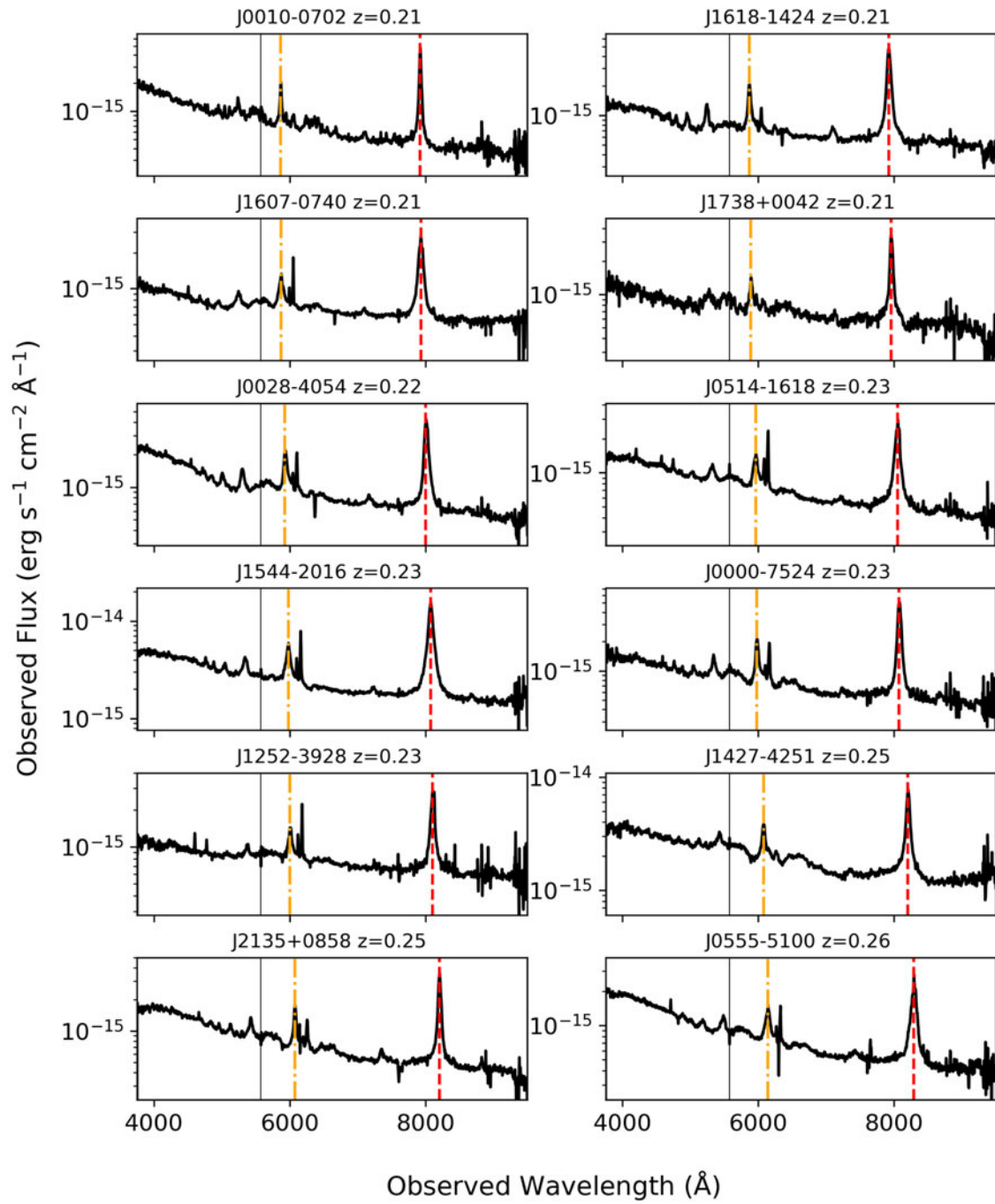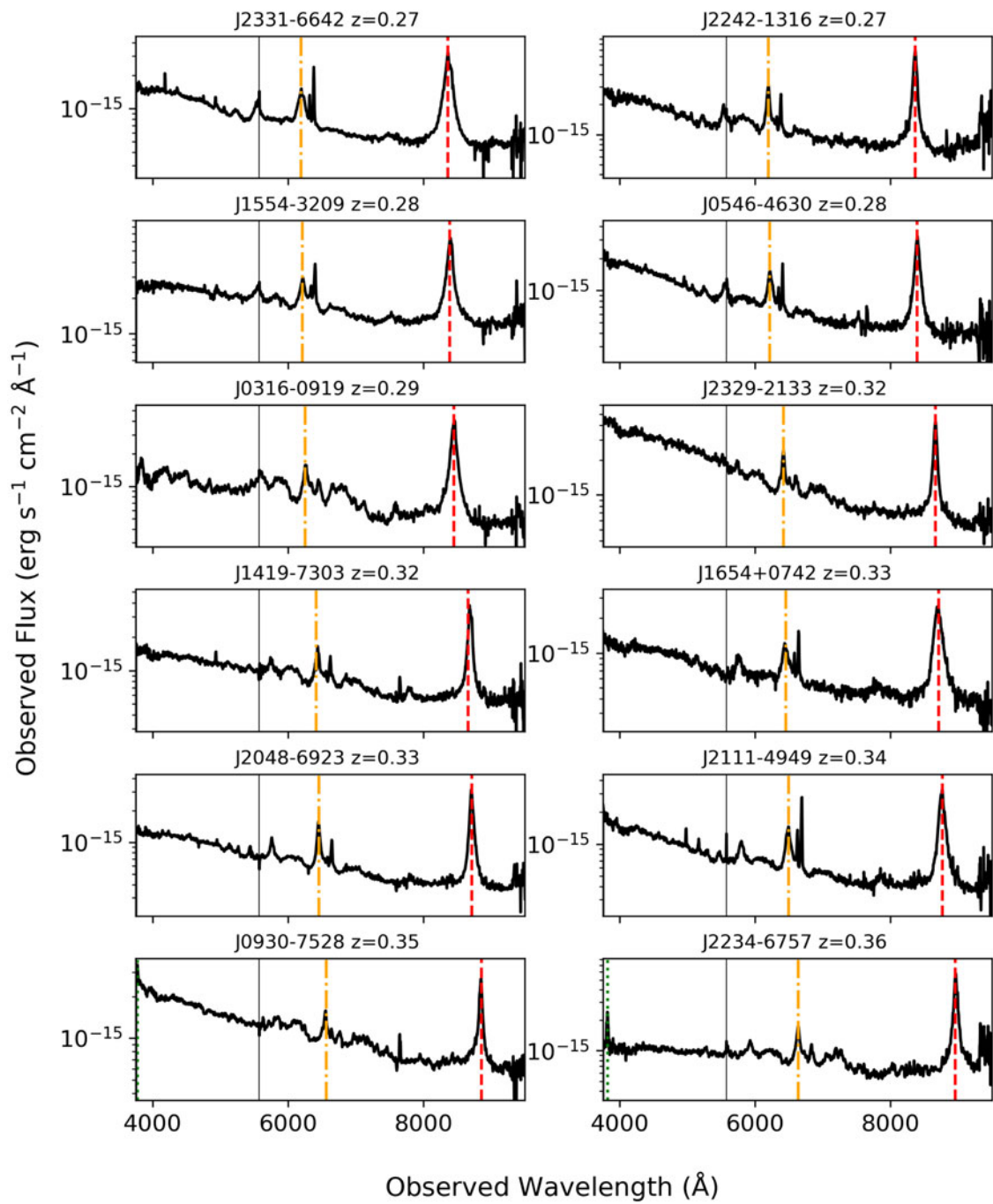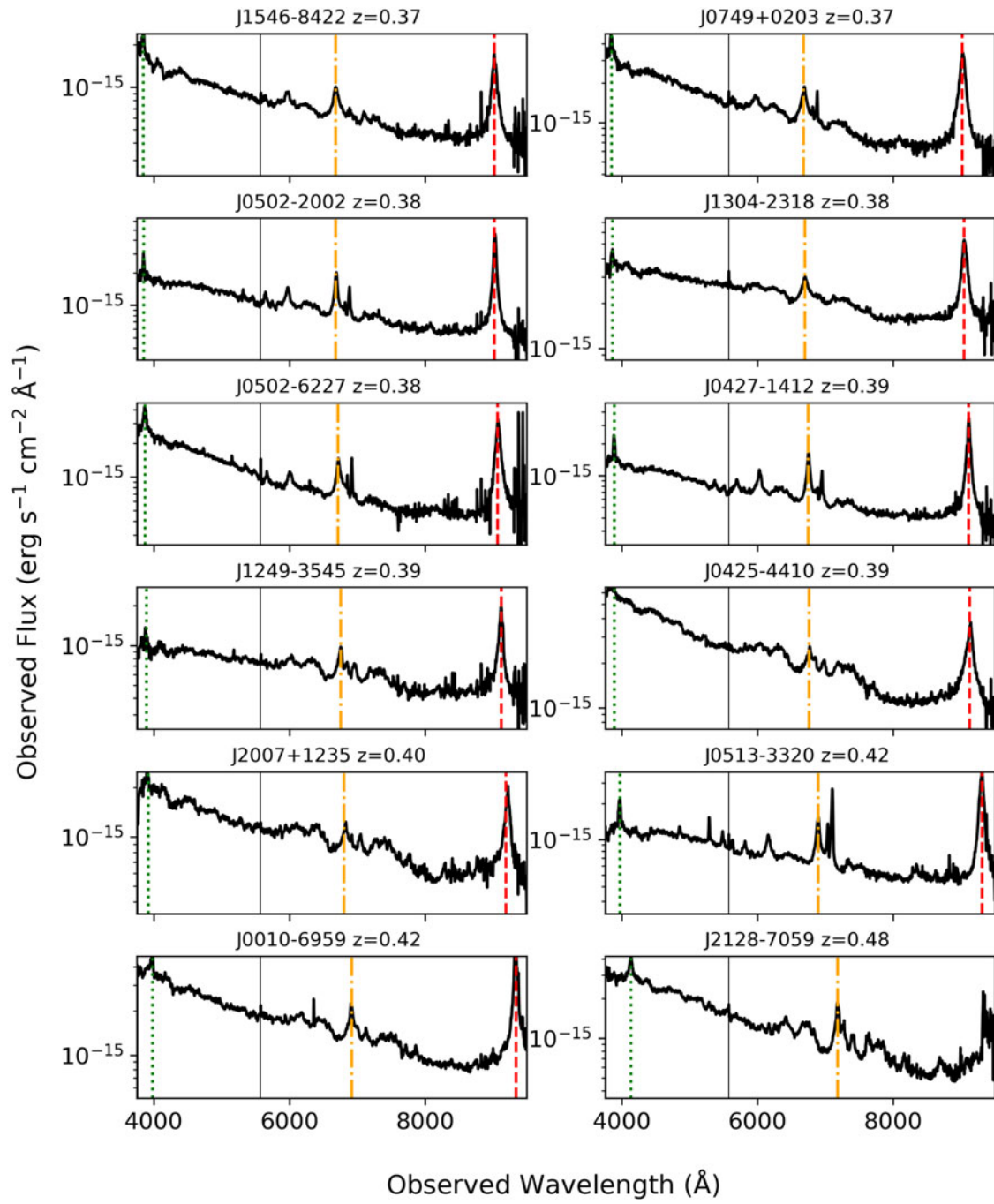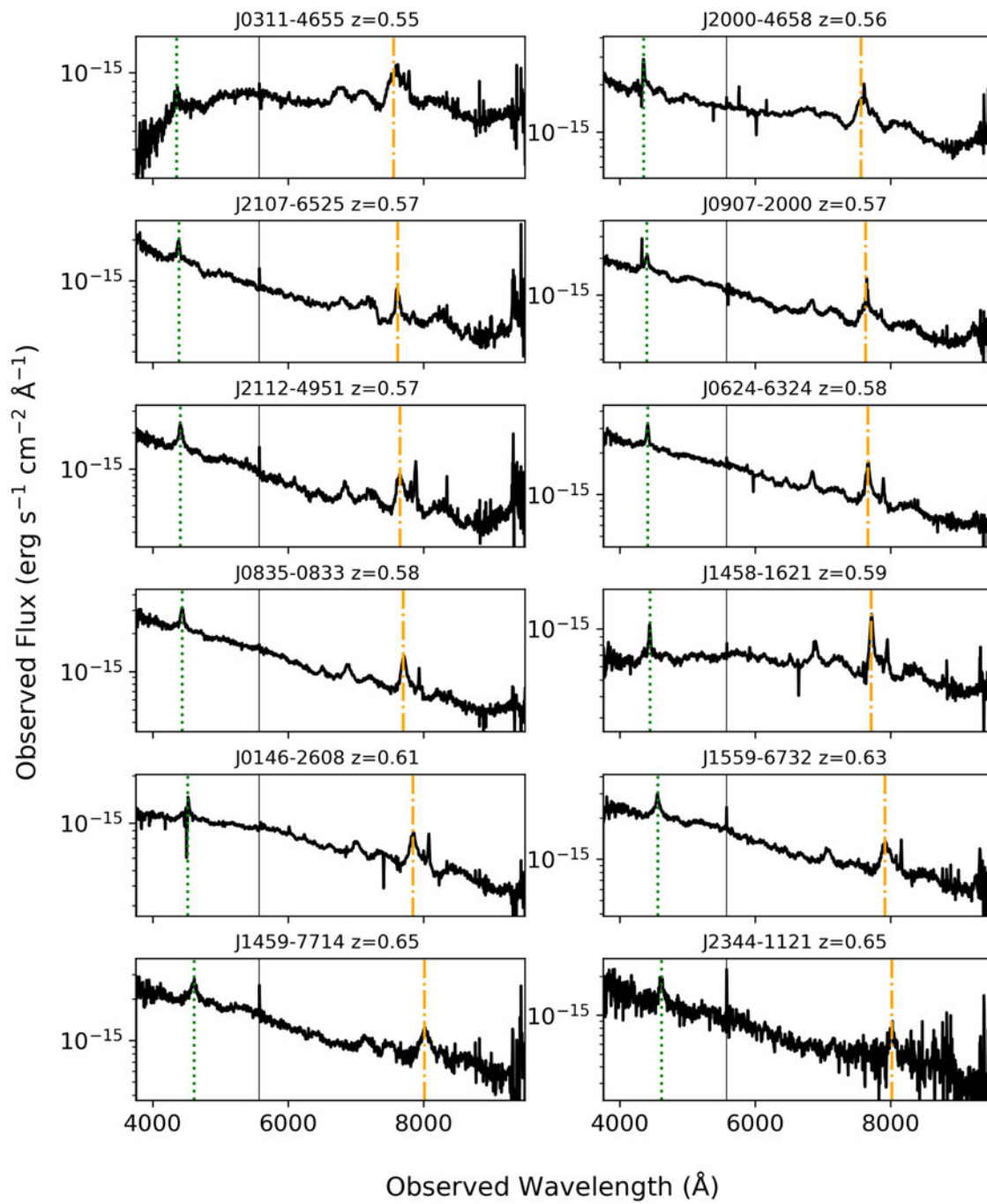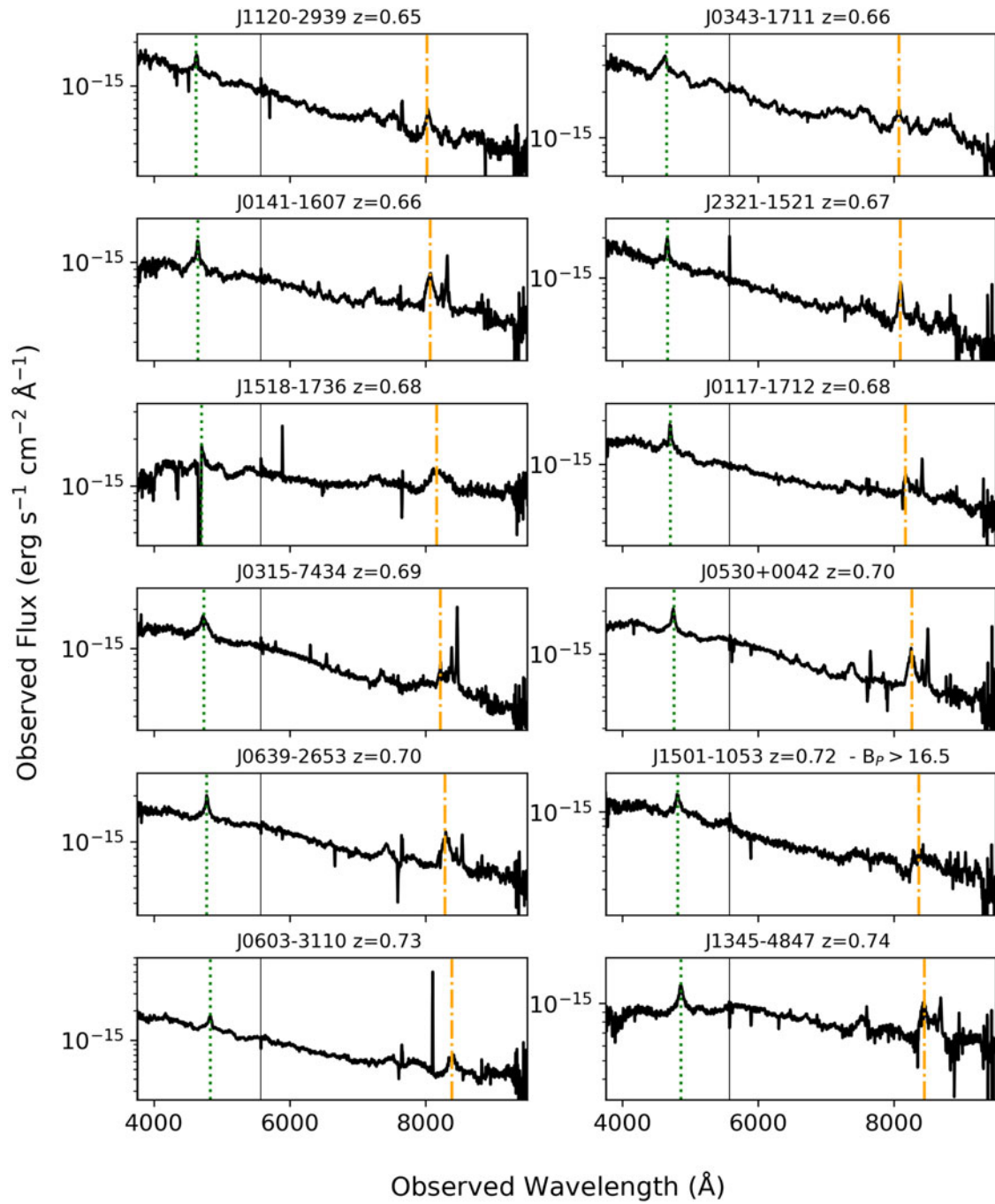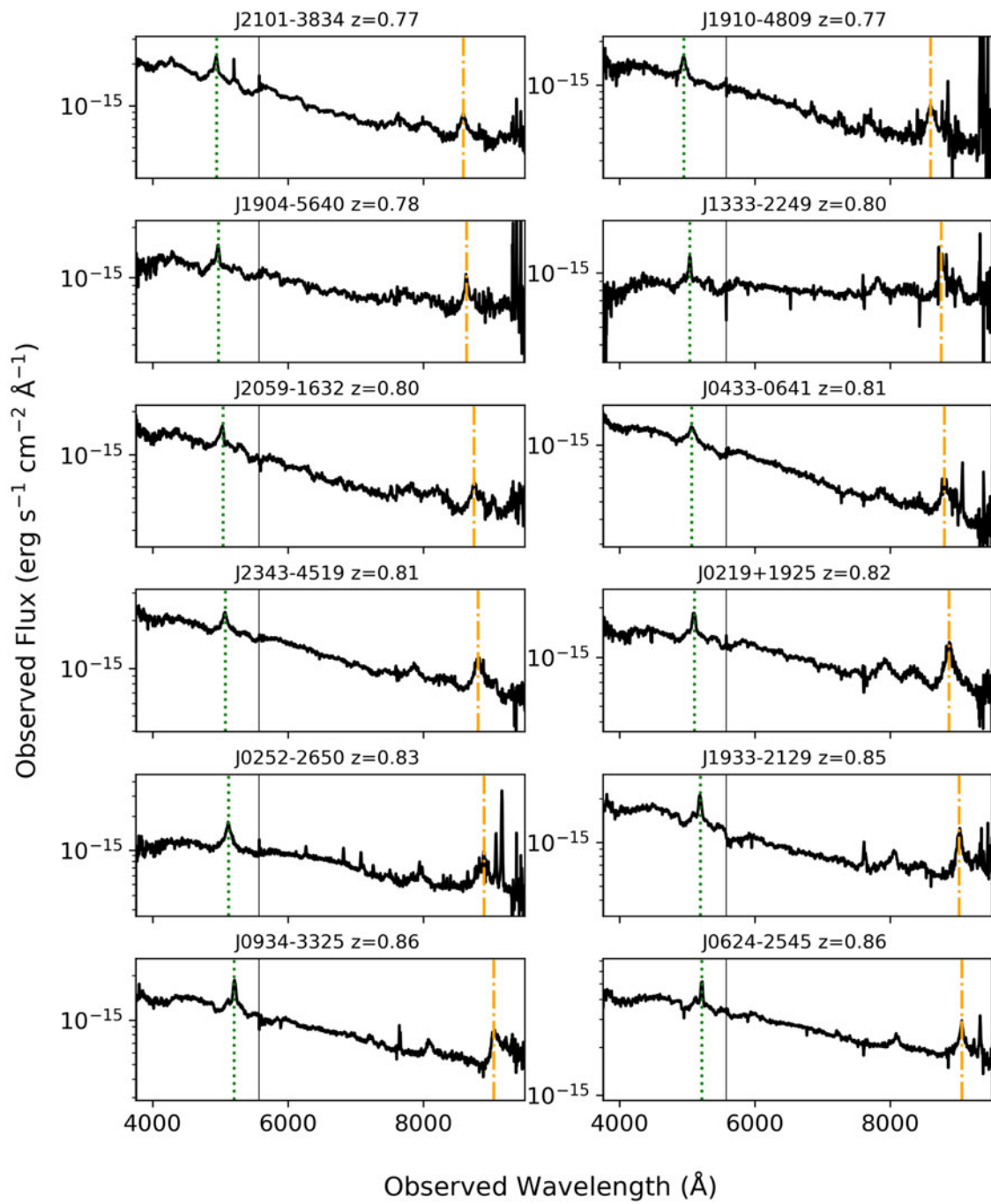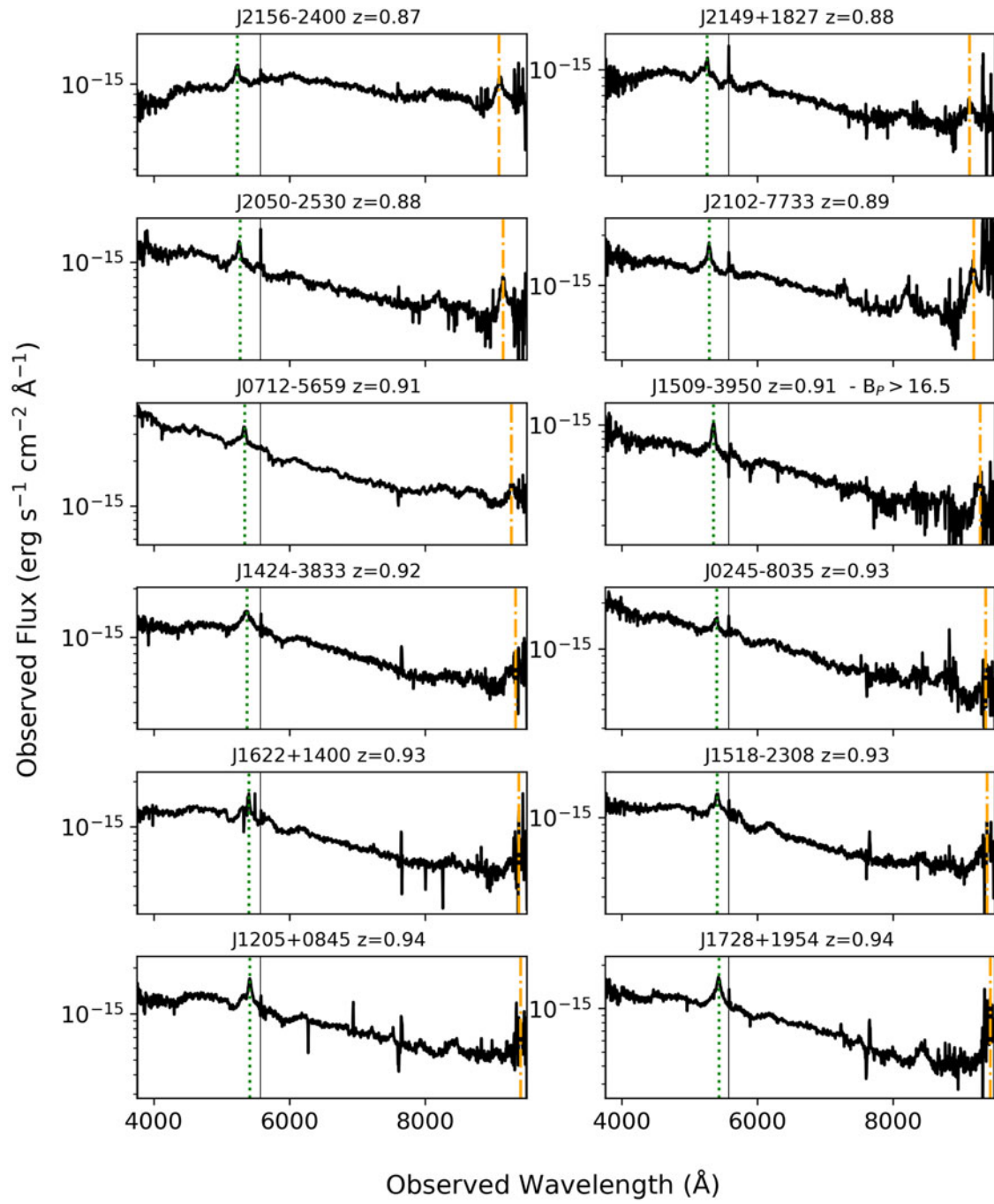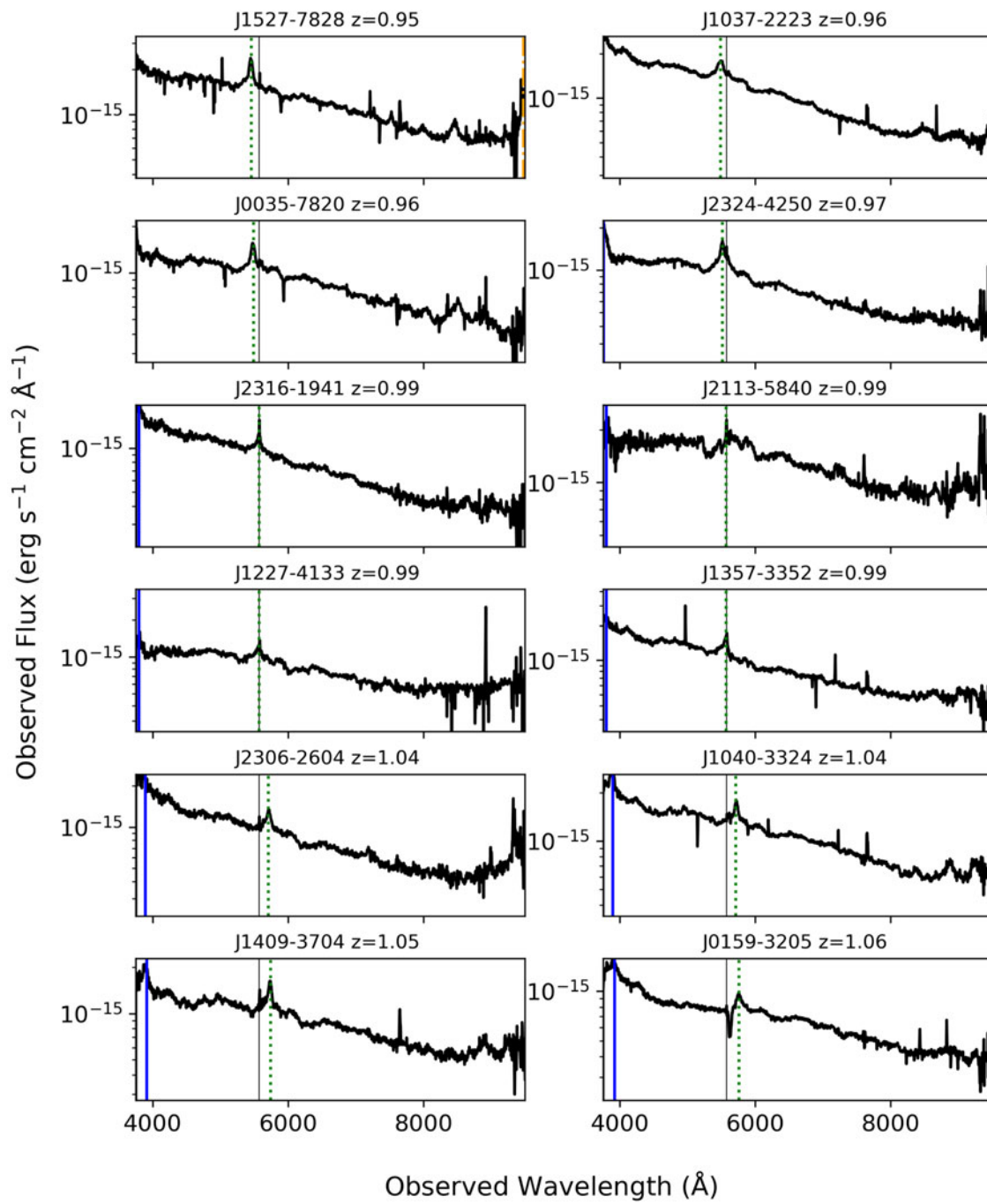
In Table D.1, we present a list of the stars observed in AllBRICQS.
Column definitions as in Appendix A. We also present the WiFeS
spectra for the stars in Figure D.1.

Table D.1. AllBRICQS stars.

Name	*Gaia* DR3 SOURCE_ID	RA (J2000)	Dec (J2000)	B_P	R_P	$W1 - W2$	UVQS	*Gaia*	Notes
		deg	deg	mag	mag	mag			
J0317+1620	55225724579988736	49.4853	16.3446	16.77	15.81	0.38	–	––	
J0423+0921	3299580282664334848	65.9506	9.3590	17.07	15.80	0.33	–	––	
J0438+0347	3281266404675233280	69.6230	3.7839	16.34	15.83	0.25	–	v–	
J0606-3113	2896198393037594112	91.6284	−31.2207	16.07	15.04	1.72	–	G–	
J1513-3109	6210717877628312448	228.4751	−31.1584	16.22	15.13	0.30	–	––	
J1908-1408	4197369116320824064	287.0005	−14.1379	17.12	15.99	0.51	–	––	

Position information from Gaia DR3.
Column definitions as in Table A.1
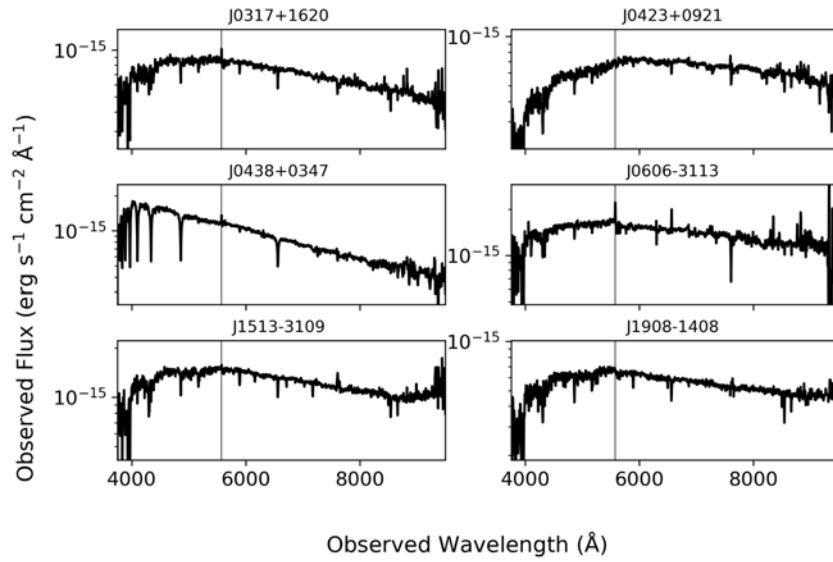
Figure D.1. WiFeS spectra of the stars observed in AllBRICQS. The y-axis shows the flux on a logarithmic scale, normalised using their Gaia DR3 photometry. The thin, black vertical line at 5575 Å indicates where the blue and red arms of the spectrograph are spliced together.

Appendix E. AllBRICQS Luminosities

In Table E.1, we list the continuum and bolometric luminosities for the confirmed AllBRICQS quasars, arranged in order of ascending RA.

Table E.1. AllBRICQS quasar luminosities.

| Name	$\log L(1450\,\text{Å})$	$\log L(3000\,\text{Å})$	$\log L(5100\,\text{Å})$	$\log L_{\text{bol}}$	Name	$\log L(1450\,\text{Å})$	$\log L(3000\,\text{Å})$	$\log L(5100\,\text{Å})$	$\log L_{\text{bol}}$
	erg s^{-1}	erg s^{-1}	erg s^{-1}	erg s^{-1}		erg s^{-1}	erg s^{-1}	erg s^{-1}	erg s^{-1}
J0000-7524	. . .	. . .	44.86	45.68	J0327-7224	. . .	. . .	44.51	45.36
J0006-6457	47.02	46.99	. . .	47.48	J0328-6225	. . .	. . .	44.81	45.63
J0010-0702	. . .	. . .	44.72	45.55	J0343-1711	. . .	46.54	46.34	47.07
J0010-6959	. . .	45.96	45.78	46.53	J0400-2257	. . .	. . .	44.64	45.48
J0014-2235	. . .	46.83	. . .	47.39	J0405-2410	. . .	46.68	. . .	47.24
J0028-4054	. . .	. . .	44.88	45.70	J0425-4410	. . .	46.06	45.81	46.59
J0035-7820	. . .	46.50	. . .	47.06	J0427-1412	. . .	45.51	45.33	46.10
J0056+1141	. . .	46.93	. . .	47.48	J0431-0838	47.31	. . .	. . .	47.67
J0117-1712	. . .	46.09	46.01	46.70	J0433-0641	. . .	46.24	45.93	46.74
J0123+0938	47.27	. . .	. . .	47.64	J0500-6322	. . .	46.79	. . .	47.35
J0140-0653	. . .	. . .	44.85	45.67	J0502-2002	. . .	45.56	45.42	46.17
J0141-1607	. . .	45.90	45.89	46.55	J0502-6227	. . .	45.69	45.34	46.20
J0146-2608	. . .	45.90	45.79	46.50	J0504+0055	47.66	. . .	. . .	47.99
J0154-5559	47.45	47.22	. . .	47.78	J0513-3320	. . .	45.49	45.42	46.14
J0159-3205	. . .	46.45	. . .	47.02	J0514-1618	. . .	. . .	44.88	45.70
J0201+1134	. . .	. . .	44.81	45.63	J0529-4351	47.88	. . .	. . .	48.19
J0207-2354	. . .	. . .	44.50	45.35	J0530+0042	. . .	46.32	46.06	46.83
J0210-5321	. . .	46.86	. . .	47.42	J0533-1434	. . .	. . .	44.57	45.41
J0219+1925	. . .	46.58	46.33	47.09	J0546-4630	. . .	45.35	45.03	45.89
J0220-2519	. . .	47.15	. . .	47.70	J0555-5100	. . .	45.31	44.99	45.85
J0241-1719	. . .	. . .	44.80	45.62	J0600-4105	. . .	46.82	. . .	47.38
J0245-8035	. . .	46.58	. . .	47.14	J0603-3110	. . .	46.20	45.94	46.72
J0252-2650	. . .	46.25	46.14	46.83	J0624-2545	. . .	46.90	46.79	47.45

Table E.1. Continued.

Name	log L(1450 Å) erg s^{-1}	log L(3000 Å) erg s^{-1}	log L(5100 Å) erg s^{-1}	log L_{bol} erg s^{-1}	Name	log L(1450 Å) erg s^{-1}	log L(3000 Å) erg s^{-1}	log L(5100 Å) erg s^{-1}	log L_{bol} erg s^{-1}
J0311-4655	. . .	45.62	45.83	46.42	J0624-6324	. . .	46.19	45.96	46.72
J0315-7434	. . .	46.16	45.97	46.71	J0634-6945	. . .	47.00	. . .	47.55
J0316-0919	. . .	45.28	45.14	45.91	J0639-2653	. . .	46.33	46.15	46.88
J0712-5659	. . .	46.84	. . .	47.40	J1409-3704	. . .	46.60	. . .	47.16
J0715-4951	. . .	. . .	44.99	45.80	J1410-3824	46.86	46.79	. . .	47.31
J0749+0203	. . .	45.75	45.52	46.31	J1416-1330	. . .	46.49	. . .	47.05
J0818-7933	. . .	46.95	. . .	47.50	J1419-7303	. . .	45.55	45.38	46.15
J0833-0628	. . .	46.72	. . .	47.28	J1422-2453	. . .	46.80	. . .	47.36
J0835-0833	. . .	46.16	45.88	46.68	J1424-3833	. . .	46.48	. . .	47.05
J0854-0718	. . .	46.71	. . .	47.27	J1427-4251	. . .	45.66	45.47	46.24
J0907-2000	. . .	46.17	45.88	46.68	J1455-4744	. . .	. . .	45.11	45.91
J0930-7528	. . .	45.71	45.51	46.28	J1458-1621	. . .	45.80	45.85	46.49
J0934-3325	. . .	46.48	46.37	47.05	J1459-7714	. . .	46.39	46.11	46.89
J1037-2223	. . .	46.59	. . .	47.15	J1501-1053	. . .	46.17	46.02	46.74
J1040-3324	. . .	46.70	. . .	47.26	J1509-3950	. . .	46.23	. . .	46.80
J1048-3401	. . .	46.83	. . .	47.39	J1518-1736	. . .	46.25	46.27	46.90
J1049-3001	. . .	46.77	. . .	47.33	J1518-2308	. . .	46.52	. . .	47.08
J1120-2939	. . .	46.08	45.82	46.61	J1527-7828	. . .	46.70	. . .	47.26
J1128-7435	. . .	47.34	. . .	47.88	J1538-4004	. . .	. . .	44.61	45.45
J1205+0845	. . .	46.43	. . .	47.00	J1544-2016	. . .	. . .	45.44	46.21
J1215-3221	. . .	. . .	44.63	45.47	J1546-8422	. . .	45.61	45.37	46.17
J1227-4133	. . .	46.49	. . .	47.05	J1547-1449	. . .	46.86	. . .	47.42
J1249-3545	. . .	45.40	45.37	46.07	J1554-3209	. . .	45.66	45.53	46.27
J1252-3928	. . .	. . .	44.97	45.78	J1559-6732	. . .	46.31	46.06	46.83
J1304-2318	. . .	46.06	45.96	46.66	J1601-7202	. . .	. . .	44.54	45.39
J1333-2249	. . .	46.22	46.33	46.92	J1607-0740	. . .	. . .	44.88	45.70
J1345-4847	. . .	46.23	46.19	46.85	J1612-6958	. . .	46.97	. . .	47.52
J1350-2924	. . .	46.55	. . .	47.11	J1618-1424	. . .	. . .	45.03	45.83
J1357-3352	. . .	46.52	. . .	47.08	J1618-3059	. . .	. . .	44.16	45.04
J1619-7832	. . .	. . .	44.63	45.47	J2102-7733	. . .	46.58	. . .	47.14
J1622+1400	. . .	46.46	. . .	47.03	J2107-6525	. . .	45.90	45.72	46.47
J1654+0742	. . .	45.40	45.21	45.99	J2111-4949	. . .	45.35	45.14	45.94
J1705+1354	. . .	46.85	. . .	47.41	J2112-4951	. . .	45.95	45.68	46.48
J1720+1115	. . .	. . .	44.91	45.72	J2113-5840	. . .	46.73	. . .	47.29
J1726+0128	47.07	47.05	. . .	47.53	J2114+1637	. . .	46.85	. . .	47.41
J1728+1954	. . .	46.46	. . .	47.03	J2116-5931	47.03	46.99	. . .	47.48
J1738+0042	. . .	. . .	45.03	45.83	J2119-0929	. . .	46.85	. . .	47.41
J1817-4144	. . .	. . .	44.83	45.65	J2126-4529	. . .	. . .	44.43	45.29
J1904-1706	. . .	. . .	45.11	45.91	J2128-7059	. . .	46.03	45.69	46.53
J1904-5640	. . .	46.31	46.26	46.92	J2135+0858	. . .	45.16	44.92	45.75
J1905-2639	. . .	. . .	44.65	45.49	J2149+1827	. . .	46.38	. . .	46.95
J1910-4809	. . .	46.25	46.09	46.81	J2156-2400	. . .	46.40	. . .	46.97
J1916-1842	. . .	. . .	44.45	45.30	J2207-1654	. . .	. . .	44.24	45.11

Table E.1. Continued.

Name	log L(1450 Å) erg s^{-1}	log L(3000 Å) erg s^{-1}	log L(5100 Å) erg s^{-1}	log L_{bol} erg s^{-1}	Name	log L(1450 Å) erg s^{-1}	log L(3000 Å) erg s^{-1}	log L(5100 Å) erg s^{-1}	log L_{bol} erg s^{-1}
J1933-2129	. . .	46.48	46.42	47.07	J2234-6757	. . .	45.30	45.39	46.05
J2000-4658	. . .	46.06	46.04	46.70	J2242-1316	. . .	45.50	45.24	46.06
J2006+1032	. . .	47.30	. . .	47.84	J2248-2446	. . .	46.89	. . .	47.44
J2007+1235	. . .	45.87	45.64	46.42	J2306-2604	. . .	46.48	. . .	47.05
J2034-0405	. . .	. . .	44.32	45.19	J2316-1941	. . .	46.43	. . .	47.00
J2048-6923	. . .	45.30	45.14	45.91	J2320-0524	. . .	46.93	. . .	47.48
J2050-2530	. . .	46.34	. . .	46.91	J2321-1521	. . .	46.09	45.84	46.62
J2055-4014	. . .	47.28	. . .	47.83	J2324-4250	. . .	46.41	. . .	46.98
J2058-1452	. . .	. . .	44.62	45.46	J2329-2133	. . .	45.75	45.39	46.26
J2059-1632	. . .	46.29	46.08	46.83	J2331-6642	. . .	45.20	45.02	45.81
J2101+1350	. . .	46.81	. . .	47.37	J2343-4519	. . .	46.45	46.30	47.00
J2101-3834	. . .	46.33	46.15	46.88	J2344-1121	. . .	46.00	45.86	46.58